Atmos. Chem. Phys. Discuss., 15, 14783–14841, 2015
www.atmos-chem-phys-discuss.net/15/14783/2015/
doi:10.5194/acpd-15-14783-2015

Atmospheric Chemistry and Physics Discussions

Global HCFC-22 measurements with MIPAS: retrieval, validation, climatologies and trends

M. Chirkov[1], G. P. Stiller[1], A. Laeng[1], S. Kellmann[1], T. von Clarmann[1], C. Boone[2], J. W. Elkins[3], A. Engel[4], N. Glatthor[1], U. Grabowski[1], C. M. Harth[5], M. Kiefer[1], F. Kolonjari[6], P. B. Krummel[7], A. Linden[1], C. R. Lunder[8], B. R. Miller[3], S. A. Montzka[3], J. Mühle[5], S. O'Doherty[9], J. Orphal[1], R. G. Prinn[10], G. Toon[11], M. K. Vollmer[12], K. A. Walker[2,6], R. F. Weiss[5], A. Wiegele[1], and D. Young[9]

[1]Karlsruhe Institute of Technology (KIT), Institute of Meteorology and Climate Research (IMK), Karlsruhe, Germany
[2]University of Waterloo, Department of Chemistry, Waterloo, Ontario, Canada
[3]NOAA/ESRL Climate Monitoring Division, Boulder, CO, USA
[4]Goethe-Universität Frankfurt, Experimental Atmospheric Research Institute for Atmospheric and Environmental Sciences, Frankfurt, Germany
[5]Scripps Institution of Oceanography, University of California, San Diego, La Jolla, CA, USA
[6]University of Toronto, Department of Physics, Toronto, Ontario, Canada
[7]CSIRO Oceans & Atmosphere Flagship, Aspendale, Victoria, Australia
[8]Norwegian Institute for Air Research, Kjeller, Norway

[9]Atmospheric Chemistry Research Group, School of Chemistry, University of Bristol, Bristol, UK
[10]Center for Global Change Science, MIT, Cambridge, MA, USA
[11]Jet Propulsion Laboratory and California Institute of Technology, Pasadena, CA, USA
[12]Laboratory for Air Pollution and Environmental Technology, Empa, Swiss Federal Laboratories for Materials Science and Technology, Dübendorf, Switzerland

Received: 10 April 2015 – Accepted: 27 April 2015 – Published: 27 May 2015

Correspondence to: G. Stiller (gabriele.stiller@kit.edu)

Published by Copernicus Publications on behalf of the European Geosciences Union.

ACPD
15, 14783–14841, 2015

Abstract

We report on HCFC-22 data acquired by the Michelson Interferometer for Passive Atmospheric Sounding (MIPAS) in reduced spectral resolution nominal mode in the period from January 2005 to April 2012 from version 5.02 level-1b spectral data and covering an altitude range from the upper troposphere (above cloud top altitude) to about 50 km. The profile retrieval was performed by constrained nonlinear least squares fitting of measured limb spectral radiances to modelled spectra. The spectral ν_4-band at $816.5 \pm 13\,\mathrm{cm}^{-1}$ was used for the retrieval. A Tikhonov-type smoothing constraint was applied to stabilise the retrieval. In the lower stratosphere, we find a global volume mixing ratio of HCFC-22 of about 185 pptv in January 2005. The linear growth rate in the lower latitudes lower stratosphere was about 6 to 7 $\mathrm{pptv\,yr}^{-1}$ in the period 2005–2012. The obtained profiles were compared with ACE-FTS satellite data v3.5, as well as with MkIV balloon profiles and in situ cryosampler balloon measurements. Between 13 and 22 km, average agreement within −3 to +5 pptv (MIPAS–ACE) with ACE-FTS v3.5 profiles is demonstrated. Agreement with MkIV solar occultation balloon-borne measurements is within 10–20 pptv below 30 km and worse above, while in situ cryosampler balloon measurements are systematically lower over their full altitude range by 15–50 pptv below 24 km and less than 10 pptv above 28 km. Obtained MIPAS HCFC-22 time series below 10 km altitude are shown to agree mostly well to corresponding time series of near-surface abundances from NOAA/ESRL and AGAGE networks, although a more pronounced seasonal cycle is obvious in the satellite data, probably due to tropopause altitude fluctuations and subsidence of polar winter stratospheric air into the troposphere. A parametric model consisting of constant, linear, quasi-biennial oscillation (QBO) and several sine and cosine terms with different periods has been fitted to the temporal variation of stratospheric HCFC-22 for all 10° latitude/1 to 2 km altitude bins. The relative linear variation was always positive, with relative increases of 40–70 % decade^{-1} in the tropics and global lower stratosphere, and up to 120 % decade^{-1} in the upper stratosphere of the northern polar region and the southern extratropical

ACPD
15, 14783–14841, 2015

hemisphere. In the middle stratosphere between 20 and 30 km, the observed trend is not consistent with the age of stratospheric air-corrected trend at ground, but stronger positive at the Southern Hemisphere and less strong increasing in the Northern Hemisphere, hinting towards changes in the stratospheric circulation over the observation period.

1 Introduction

HCFC-22 (CHF_2Cl) is a chlorine source gas and a greenhouse gas. Sources of HCFC-22 are anthropogenic emissions due to its use as a propellant and refrigerant. The gas is removed from the atmosphere by photolysis and by reaction with the OH radical. The chemical lifetime of HCFC-22 in the stratosphere is 161 years (12 years for its global total atmospheric lifetime), according to World Meteorological Organization (WMO), but has been estimated to a significantly longer span of 260 ± 25 years by Moore and Remedios (2008). The radiative forcing potential of HCFC-22 is $0.208\,W\,m^{-2}\,ppbv^{-1}$, and its ozone depletion potential is about 20 times lower than that of CFC-12 (0.04) (World Meteorological Organization , WMO). Production and import of HCFC-22 is limited by the Montreal Protocol on Substances that Deplete the Ozone Layer and will be banned by 2030 for dispersive uses in developed countries (United Nations Environment Programme, 2009). The 2007 Amendment to the Protocol asks for a 100 % reduction by 2030 also for developing countries – albeit with a 2.5 % allowance for servicing of refrigeration and air conditioning equipment existing on 1 January 2030 for the period 2030–2040 and subject to review in 2015. So the overall reduction shall already be 97.5–100 % by 2030.

Ambient HCFC-22 was first measured by Rasmussen et al. (1980) by in situ techniques. Atmospheric HCFC-22 abundances are typically measured on site by gas-chromatographic techniques or by collecting samples in flasks followed by subsequent gas-chromatographic analysis in a central laboratory (Montzka et al., 2009; O'Doherty et al., 2004; Yokouchi et al., 2006) or by balloon-borne air-sampling measurements (En-

ACPD
15, 14783–14841, 2015

gel et al., 1997). Further, there exist remote measurements by infrared spectroscopy from ground-based (Rinsland et al., 2005b; Zander et al., 2005; Gardiner et al., 2008), balloon-borne (Murcray et al., 1975; Williams et al., 1976; Goldman et al., 1981), or space-borne (Zander et al., 1987; Rinsland et al., 2005a; Moore and Remedios, 2008) platforms in solar absorption geometry. Among recently flying space-borne instruments, only the Atmospheric Chemistry Experiment – Fourier Transform Spectrometer (ACE-FTS; solar occultation) and the Michelson Interferometer for Passive Atmospheric Sounding (MIPAS; limb emission) have been providing measurements of HCFC-22 (Kolonjari et al., 2012; Park et al., 2014; Moore and Remedios, 2008). The history of measurements is summarized in von Clarmann (2013).

In this paper we present and discuss HCFC-22 distributions and time series as retrieved with the MIPAS data processor developed and operated by the Institute of Meteorology and Climate Research at the Karlsruhe Institute of Technology (KIT-IMK) in Germany in cooperation with the Instituto de Astrofísica de Andalucía (IAA, CSIC) in Granada, Spain. In the next section we provide a description of the MIPAS instrument and measurements. The retrieval strategy and error estimation are summarized in Sect. 3. Section 4 reports on the validation of this data set, and Sect. 5 presents the climatology of HCFC-22 distributions and an assessment of temporal variations including a linear trend. The derived estimates of trends will be compared to those from ground-based long-term data records. Section 6 contains the discussion of the results and the summary.

2 MIPAS data

MIPAS measured the thermal emission of the atmosphere, and thus provided data during day and night. It was a cryogenic limb emission FTS designed for measurement of trace species from space (European Space Agency, 2000; Endemann and Fischer, 1993; Endemann et al., 1996; Fischer and Oelhaf, 1996). MIPAS was one of 10 instruments aboard the Environmental Satellite (Envisat). Envisat was launched

ACPD
15, 14783–14841, 2015

into a sun-synchronous polar orbit on 1 March 2002 at approximately 800 km, with an orbital period of about 101 min (Fischer et al., 2008). The end of the Envisat mission was declared on 9 May 2012 after loss of communication with the satellite on 8 April 2012.

MIPAS sounded the atmosphere tangential to the Earth in the infrared spectral range (4.15–14.6 µm) covering tangent altitudes from about 7 to 72 km in its nominal observation mode. The instrument's field of view was approximately 3 km (vertically) × 30 km (horizontally). MIPAS operated from July 2002 to March 2004 with full spectral resolution as specified: 0.05 cm^{-1} in terms of full width at half maximum, after apodisation with the "strong" function suggested by Norton and Beer (1976). The full resolution mode was stopped in March 2004. Starting from January 2005 and up to the end of the mission, the spectral resolution of MIPAS was degraded from 0.05 to 0.12 cm^{-1} (apodised). These later measurements are referred to as "reduced resolution mode".

The data analysis reported in this paper relies on the ESA-provided so-called level-1B data product which includes calibrated phase-corrected and geolocated radiance spectra (Nett et al., 1999). The versions of ESA level-1B data used are IPF 5.02–5.06. All spectra under consideration here were recorded according to the nominal reduced resolution measurement mode, including per limb sequence 27 tangent altitudes between about 7 and 72 km, with the tangent altitude adjustment following roughly the tropopause altitude over latitudes. The vertical distance between adjacent tangent heights varies between 1.5 km in the upper troposphere/lower stratosphere up to 4.5 km in the mesosphere.

3 Retrieval

The retrievals of HCFC-22 profiles presented here were performed with a MIPAS data processor dedicated for research applications, which has been developed at the Institute of Meteorology and Climate Research (IMK) and complemented by components

ACPD
15, 14783–14841, 2015

relevant to treatment of non-local thermodynamic equilibrium at the Instituto de Astrofísica de Andalucía (IAA). The non-LTE components are not used in this study because they are not relevant to the retrieval of HCFC-22.

The IMK retrieval processor consists of the radiative transfer algorithm KOPRA (Stiller, 2000) and the retrieval algorithm RCP (Retrieval Control Program). Local spherical homogeneity of the atmosphere is assumed here, i.e., atmospheric state parameters related to one limb sounding sequence are assumed not to vary with latitude or longitude but only with altitude. An exception is temperature for which horizontal gradients are considered in the retrieval (Kiefer et al., 2010). The general strategy of the IMK/IAA data processing has been documented in von Clarmann et al. (2003).

3.1 Retrieval of HCFC-22

HCFC-22 is retrieved by constrained multi-parameter non-linear least-squares fitting of modelled to measured spectra. Spectral data from all tangent altitudes are analysed within one inversion process, as suggested by Carlotti (1988). Volume mixing ratio (vmr) vertical profiles are retrieved on a fixed, i.e. tangent height independent altitude grid which is finer than the tangent height spacing (1 km steps from 4 to 35 km; then 5 km grid width from 35 to 50 km; 10 km grid width from 50 to 100 km; 120 km). In order to obtain stable profiles, the profiles have been constrained such that the first order finite difference quotient Δvmr/Δaltitude at adjacent altitude grid points was minimised, similar as proposed by Tikhonov (1963). An altitude-constant zero-level profile was taken as a priori, while the initial guess profile was from the MIPAS climatology (Kiefer et al., 2002). For the retrieval of HCFC-22 we have used 4 micro windows of the MIPAS spectrum (803.500 to 804.750, 808.250 to 809.750, 820.500 to 821.125 and 828.750 to 829.500 cm^{-1}).

Figure 1 shows the atmospheric limb emission radiance spectrum at 16 km tangent altitude including contributions from H_2O, CO_2, O_3, NO_2, NH_3, HNO_3, ClO, OCS, HCN, CH_3Cl, C_2H_2, C_2H_6, COF_2, C_2H_4, HNO_4, CFC-11, CCl_4, CFC-113, $ClONO_2$, CH_3CCl_3,

ACPD
15, 14783–14841, 2015

CH_3OH, $C_2H_3NO_5$ (peroxyacetyl nitrate, PAN), C_3H_6O and HCFC-22 (black curve). In addition, the contribution of HCFC-22 is shown (red curve).

The following information from preceding retrieval steps was used for the retrieval of HCFC-22: a correction of the spectral shift caused by less-than-perfect frequency calibration, tangent height and temperature, and the species O_3, H_2O, HNO_3, ClO, $ClONO_2$, CFC-11, HNO_4 and C_2H_6. The vmr of CO_2 and all other remaining gases are taken from a climatological database, and the temperature was retrieved from CO_2 lines.

Simultaneously with HCFC-22 and with adequate regularisation, we jointly fit PAN, a wavenumber-independent radiation background per microwindow attributed to aerosol emission, and an additive radiative offset for each micro-window. The data versions are V5r_F22_220 and V5r_F22_221. The only difference between these versions is the source of temperature analysis data used as a priori for the preceding temperature retrieval. Results are equivalent and different version numbers are used only to guarantee full traceability of the retrievals.

3.2 Diagnostics

Diagnostic quantities to characterize the HCFC-22 measurements include estimates of measurement noise, of retrieval errors caused by uncertainties in ancillary parameters used in the radiative transfer modelling, and the averaging kernel (AK) matrix (Rodgers, 2000).

Table 1 shows the estimated total retrieval error of a HCFC-22 profile measured at 18.6° S and 111.6° W on 9 January 2009. The total error is the square root of the quadratic sum of noise error and parameter errors. Its dominating components are the uncertainty of the elevation pointing of the line of sight (LOS), the uncertainty of pre-retrieved O_3 mixing ratios, the gain calibration uncertainty, the residual spectral shift uncertainty, and the instrument line shape (ILS) uncertainty. The spectroscopic error (not reported in the table) is about 5 %. In the given altitude range, errors resulting from uncertainties of interfering species contribute to the total error by less than 1 %.

ACPD
15, 14783–14841, 2015

The percentage of non-converged profiles is about 0.01 to 0.02 %. The strength of the regularization has been chosen altitude-dependent with a scheme proposed by Steck (2002) such that the retrieved profile represents approximately 5° of freedom, corresponding to a typical altitude resolution of 3 km at 10 km height and 7 km at 30 km height, and further increasing with height (Fig. 2). Here the vertical resolution is provided in terms of full width at half maximum of a row of the averaging kernel matrix. The rows of the AK-matrix show how much information from other atmospheric altitudes contribute to the vmr on the given retrieval altitude. An example of the rows of the HCFC-22 averaging kernel matrix is shown in Fig. 3. The largest peaks of the averaging kernels are generally found in the upper troposphere. This is because the retrieval is more strongly regularised at higher altitudes. In general, the retrieval is well-behaved in a sense that the averaging kernels peak at their nominal altitudes (marked by diamonds in Fig. 3) between 12 and 50 km.

The information evaluated by a limb retrieval is not located in one single point but spread horizontally along the line of sight direction. The horizontal information smearing of the HCFC-22 measurement is estimated by using the method of von Clarmann et al. (2009). In terms of full width at half maximum of the rows of the horizontal averaging kernel matrix, the horizontal information smearing of a MIPAS retrieval typically varies between about 210 and 680 km for most species, altitudes and atmospheric conditions. For HCFC-22 the horizontal information smearing, calculated as the half width of the horizontal component of the 2-D averaging kernel, is approximately 300 km at altitudes below 15 km, 608 km at altitude 20 km and approximately 550 km above (see Table 2).

The information displacement is defined as the horizontal distance between the point where the most information comes from and the nominal geolocation of the limb scan, which is defined as the geolocation of the tangent point of the middle line of sight in a MIPAS limb scan. The information displacement in case of HCFC-22 varies between −121 km at 40 km altitude (the negative sign refers to displacement beyond the tangent

ACPD
15, 14783–14841, 2015

point with respect to the satellite) and 133 km at 15 km altitude, and is lowest and positive (i.e. displacement towards the satellite) in the middle stratosphere (see Table 2).

4 Validation

Validation of the HCFC-22 MIPAS IMK profiles is performed by comparison to coincident independent measurements. The availability of reference measurements for the validation of MIPAS HCFC-22 in the stratosphere is quite limited: the only spaceborne instrument measuring the vertical profiles of HCFC-22 at the same time as MIPAS is ACE-FTS. We also perform the comparison with MkIV balloon profiles and with measurements at different heights performed with the balloon-borne cryosampler flown by the University of Frankfurt. Although there exist aircraft air measurements of HCFC-22 (e.g. Xiang et al., 2014), these have not been used, because of unsolved problems caused by the different altitude resolutions of MIPAS and the air sampling measurements.

4.1 Comparison with ACE-FTS

The Atmospheric Chemistry Experiment Fourier Transform Spectrometer (ACE-FTS) is a solar occultation instrument flying on the SCISAT satellite platform since August 2003 (Bernath et al., 2005). It takes measurements from the upper troposphere to about 150 km altitude. Temperature, pressure, atmospheric aerosol extinction, and the concentrations of a large number of atmospheric species are retrieved from these measurements with a vertical resolution in the order of 4 km. The SCISAT flies on a highly inclined circular orbit (650 km altitude), which implies that more than half of the ACE-FTS measurements occur at high (over 60° N and S) latitudes.

HCFC-22 is retrieved by the algorithm described in Boone et al. (2005) and Boone et al. (2013) from a single window of width 25 cm^{-1} centered at 817.5 cm^{-1}. The ACE-FTS retrieved HCFC-22 profiles extend from the upper troposphere to about 30 km

ACPD
15, 14783–14841, 2015

height, do not include any formal a priori information, and the reported errors are in the order of 3 to 5 %, going up to 10 % at the lowest and 8 % at the highest altitude limits of the retrieval.

The analysis was performed on January 2005–April 2012 data of ACE-FTS version 3.5, with collocation criteria of 500 km and 5 h; this leads to a comparison subset of 8393 collocated measurements. In the case of multiple matches, only the closest MIPAS profile was used.

The comparison of global mean MIPAS and ACE-FTS HCFC-22 (left panel of Fig. 4) profiles reveals a high MIPAS bias of 5 to 10 pptv at 17–29 km altitudes and a low MIPAS bias (between 0 and −3 pptv) at 10–13 km. Between 13 and 22 km altitude, the mean difference is −3 to +5 pptv. The bias is significant at all altitude levels. Analysis of the scatter of the differences vs. the estimated combined precision of the instruments (Fig. 4, right panel) indicates an underestimation of the combined uncertainty, i.e. one or both instruments underestimate the random component of their errors (c.f. von Clarmann, 2006). It should, however, be kept in mind that the reported fitting error estimates of ACE-FTS include only measurement noise and do not include randomly varying parameter errors, which implies that perfect coincidence of the two curves on the right panel of Fig. 4 cannot be expected. Further, atmospheric variability within the radius defined by the co-incidence criteria can contribute to these differences. This is particularly true because many of the ACE-FTS measurements occur at higher northern latitudes where atmospheric variability is quite pronounced.

The seasonality of the differences between ACE-FTS and MIPAS for southern polar latitudes is analysed in Fig. 5. Most pronounced differences occur at the top end of the ACE-FTS profiles, with ACE-FTS always lower than MIPAS, while the seasonality in the differences comes mainly from a very steep vertical gradient in the ACE-FTS profiles for polar summer between 16 and 20 km altitude (top left panel) which is not in the same way reproduced by MIPAS profiles. The very steep vertical gradient in this particular case leads to the highest bias of ACE-FTS vs. MIPAS of about 15 pptv around 16 km and a low bias around 20 km and above.

ACPD
15, 14783–14841, 2015

The correlation plots of ACE-FTS vs. MIPAS (Fig. 6) corroborate the findings so far: the ACE-FTS and MIPAS data points fall into two clusters that match around 16 km altitude. Below this altitude (red and yellow colors) the regression line is slightly steeper than unity indicating a bias proportional to the absolute values, while above 16 km ACE-FTS has a small and almost constant low bias vs. MIPAS.

The histogram plots (Fig. 7) represent the distribution of measured volume mixing ratios over latitude and time for a fixed altitude level. The histograms for ACE-FTS and MIPAS at 23 km are very similar in shape and position of the peak value, while at 16 km the ACE-FTS distribution of measured vmrs is somewhat wider. Nevertheless, both peak and extreme values match quite well.

In summary, although minor differences between MIPAS and ACE-FTS HCFC-22 measurements have been detected, the comparison justifies confidence in the data sets. Besides identified small biases in the order of < 10 pptv the two data sets compare very well in absolute values, latitude distributions and seasonalities.

4.2 Comparison with cryosampler profiles

The cryogenic whole air sampler, deployed on stratospheric balloons, is operated by the University of Frankfurt. The instrument collects high volume whole air samples which are frozen out by means of liquid neon. After the flight the air is left to evaporate which provides high pressure whole air samples from different altitudes (Engel et al., 1997). A wide range of halocarbons are then analyzed in these samples using a gas chromatograph (GC) coupled to a mass-spectrometer (Laube et al., 2008). The precision of the individual data points of the cryosampler measurements is typically in the order of 0.5 %. The data are reported relative to a standard provided by the National Oceanic and Atmospheric Administration (NOAA) (e.g. Montzka et al., 2003) on the NOAA-2006 scale, which shows excellent agreement (within 1 %) to most other scales (Hall et al., 2014).

Cryosampler measurements do not represent contiguous vertical profiles but rather individual independent point measurements. Hence, no regridding has been applied

ACPD
15, 14783–14841, 2015

in this case: the cryosampler measurements were just reported as they were on the height where they had been taken.

Coincidences between MIPAS and cryosampler measurements were searched for within 1000 km and 24 h. Besides the co-incident data, we compare also seasonal means from MIPAS to the cryosampler data in order to estimate how far typical situations were sounded.

For the first two flights (upper panels of Fig. 8) that took place in June 2005 in the tropics the agreement between MIPAS profiles and cryosampler measurements above 30 km altitude is better than 10 pptv. As expected, the individual co-located profiles agree better than the corresponding multi-annual seasonal zonal means to the cryosampler data. Nevertheless, the MIPAS profile with the closest coincidence differs significantly from the other coincident profiles in both cases, hinting towards inhomogeneous situations in the atmosphere. Below 30 km, for the first flight neither the closest coincident profile, nor the mean of coincidences, nor the climatological profile agrees with the cryosampler measurements. MIPAS data are higher than the cryosampler measurements between 15 pptv (mean coincident profile) and 35 pptv (closest profile). For the second flight, the cryosampler data points fall within the error bars of the closest MIPAS profile.

The third flight (middle left panel of Fig. 8) of the cryosampler instrument provided only four measurements, none of which being situated between 18 and 32 km. For all four data points, MIPAS is higher by 15–30 pptv. The cryosampler data of the fourth flight (bottom right panel) show some oscillations around the closest MIPAS profile between 20 and 30 km altitude, which are not resolved by MIPAS, whose measurements represent for each profile point an air parcel of about 400 km in length times 30 km in width times 4 km in height. The MIPAS profile lies just between the oscillating cryosampler data points. The oscillating cryosampler data are attributed to a strong variability of the atmosphere on this particular day. This hypothesis is corroborated by the large spread of the collocated MIPAS profiles. Above 24 km altitude, the cryosampler data

ACPD
15, 14783–14841, 2015

points lie within the spread of the MIPAS coincidences, while below 24 km, MIPAS profiles have a pronounced high bias of 30 to 50 pptv.

The last flight (bottom left panel of Fig. 8) stands out by a pronounced HCFC-22 minimum (also present in the profiles of other tracers measured during this flight) in MIPAS data at approximately 28 km. Below this altitude, the cryosampler measurements coincide nicely with the MIPAS data but the altitude coverage of the cryosampler data set on this day does not allow to confirm the positive mixing ratio gradient above.

In summary, comparison to cryosampler data from five different profiles from tropical and northern polar winter atmosphere reveal a high bias of MIPAS HCFC-22 data of 15 to 50 pptv below 24 km, while above 28 km, the high bias is reduced to less than 10 pptv. The analysis of the comparisons is partly complicated by very inhomogeneous atmospheric situations and the enormous difference between sampling volumes of cryosamplers vs. satellite remote sensing instruments.

4.3 Comparison with MkIV balloon interferometer profiles

The MkIV interferometer from Jet Propulsion Laboratory (JPL) is a high-resolution solar absorption spectrometer which is deployed on stratospheric balloon platforms with a typical float altitude of 37 km (Toon, 1991). MkIV measured HCFC-22 using two spectral windows, centered at the ν_4 Q-branch at 809.19 cm^{-1} and the $2\nu_6$ Q-branch at 829.14 cm^{-1}.The widths of the microwindows were 1.28 and 0.72 cm^{-1}, respectively. The instrument is designed so that the entire mid-infrared region can be observed simultaneously with good linearity and signal-to-noise ratio. In this region over 30 different gases have identifiable spectral signatures including HCFC-22. The instrument obtains vmr vertical profiles between cloud top and balloon altitude. MkIV measured three HCFC-22 vmr vertical profiles during the MIPAS reduced resolution period. The dataset is provided on an 1 km altitude grid between 10 and 40 km. The vertical resolution of the MkIV balloon profiles varies between 2–4 km. Data used here were measured during balloon flights from Fort Sumner, with tangent altitude geolocations from 34.0–35.7° N and 108.8–114.1° W.

ACPD
15, 14783–14841, 2015

Figure 9 presents the three MkIV balloon profiles within the MIPAS reduced resolution period. The first two MkIV profiles, from 20 September 2005 and 22 September 2007, were measured when MIPAS was temporarily inactive and no matches were found within 24 h and 1000 km. The MkIV profile from the 2005 flight was hence compared to the MIPAS multi-annual September 30–40° N monthly mean profile, and the MkIV profiles from 22 September 2007 was in addition compared to the MIPAS 30–40° N monthly mean of September 2007. For the profile from the sunrise of 23 September 2007, three collocated MIPAS profiles were found (grey lines).

Below 25 km MIPAS profiles agree with the MkIV profiles within the error bars, with MIPAS HCFC-22 being in tendency lower for the collocated profiles, (bottom left panel), higher for the multi-annual September mean (top left panel) and in good agreement for the September 2007 monthly mean. Above 25 km the vertical gradients of mixing ratios from MkIV and MIPAS diverge, with MkIV profiles decreasing stronger with altitude than those of MIPAS. Up to 32 km, the agreement is still well within the error bars. For the 22 September 2007 comparison the profiles agree even up to the highest MkIV altitude levels.

4.4 Summary of the intercomparisons

The comparisons to the three available reference data sets, namely ACE-FTS, balloon-borne cryosampler data, and MkIV balloon measurements, do not provide a unique picture on MIPAS biases. Below about 20 km, MIPAS has either a low (ACE-FTS), a high (cryosampler) or no (MkIV) bias. Above 25 km the MIPAS bias is either clearly positive (ACE-FTS and MkIV) or small, i.e. less than +10 pptv (cryosampler). Between 20 and 25 km the bias can range from −30 pptv (MkIV) to +50 pptv (cryosampler). In summary we state that the MIPAS HCFC-22 data are found to be within ±15 pptv (1-σ) of reference data sets between 10 and 35 km altitude.

ACPD
15, 14783–14841, 2015

5 Climatology and trends

5.1 Zonal means

Figures 10 and 11 show monthly zonal means of HCFC-22 vmr for December 2005 and 2010, and July 2006 and 2010, respectively, for all latitudes and altitudes up to 50 km. The months have been selected to be approximately in the same phase of the quasi-biennial oscillation (QBO). The typical distribution of a tropospheric source gas with photolytic sinks in the stratosphere is observed, with higher values in the tropics and lower altitudes, and lower values in the upper stratosphere and higher latitudes. At tropospheric altitudes, MIPAS sees larger HCFC-22 abundances in the Northern Hemisphere (NH) than in the Southern Hemisphere (SH), owing to the global distribution of emissions, which is in agreement with previous results from Xiang et al. (2014), while in the stratosphere this kind of asymmetry is not observed. Furthermore, a substantial increase of HCFC-22 from the year 2005/06 to the year 2010 can be derived from these figures.

The HCFC-22 distributions show a maximum in the tropical upper troposphere which is, at first glance, not expected for a source gas emitted at the ground. Highest HCFC-22 vmrs, on an absolute scale, of up to 240 pptv at the end of the observation period occur at altitudes between 10 and 15 km at 30–50° N during boreal summer (compare Fig. 14). Figure 15 for 14 km altitude demonstrates that these high amounts, probably related to the Asian monsoon anticyclone, are transported into the TTL and subsequently distributed over the tropics, providing the isolated maximum layer of up to 225 pptv in the tropics. The following scenario is suggested: high HCFC-22 abundances from industrial regions of Asian developing countries are transported upwards into the Asian monsoon anticyclone during summer. This is plausible since HCFC-22 production was not restricted for developing countries during the relevant time, and some of these countries, e.g. China, have been large HCFC producers for years, while HCFC-22 production is controlled by the Montreal protocol for industrialised countries. Indeed, Saikawa et al. (2012) found a surge in HCFC-22 emissions between 2005

ACPD
15, 14783–14841, 2015

and 2009 from developing countries in Asia with the largest emitting region including China and India. Also Montzka et al. (2009) suggested a shift from high to low latitude emissions during this period, consistent with these assertions. Hoyle et al. (2011) demonstrated that atmospheric models produce vertical profiles of chemical tracers with a local maximum just below the tropical tropopause. They explained their findings by rapid uplift of tracers due to deep convection, leaving less time for chemical conversion than outside the convective towers. This process would explain why the isolated HCFC-22 vmr maximum observed by MIPAS above about 10 km exceeds abundances measured at the surface by the Global Monitoring Division of NOAA's Earth System Research Laboratory at remote mid-latitude sites (cf. Sect. 5.4). After having been lifted into close-to-tropopause levels inside the Asian monsoon anticyclone, the high HCFC-22 abundances are transported into the tropical tropopause region. Transport from the Asian monsoon anticyclone into the tropical tropopause layer as a dominant source of tropical seasonality was suggested by Ploeger et al. (2012) based on model experiments, and by Randel and Jensen (2013). Once intruded into the TTL, the enhanced HCFC-22 abundances are distributed over all the tropics (compare Fig. 15, panel 2) and generate an isolated maximum layer between appr. 10 km and the tropopause.

5.2 Time series analysis of HCFC-22 for various altitudes and latitudes

The MIPAS HCFC-22 data presented here cover the so-called reduced-resolution phase from January 2005 to April 2012. The instrument did not measure continuously in the nominal mode. This leads to frequent data gaps, but they are relatively short on average (1 to 2 days, occasionally longer). Some days were filtered out as well, since they contain too few measurements, and for certain phases there are data gaps in certain latitudes due to calibration measurements always performed at the same latitudes.

The averaged global time series of HCFC-22 volume mixing ratio from January 2005 to April 2012, including all latitudes from the South to the North Pole is shown in Fig. 12.

ACPD
15, 14783–14841, 2015

The global mean HCFC-22 volume mixing ratio increases at all altitudes with time. The global mean HCFC-22 volume mixing ratio at, for example, 16 km altitude was about 161 pptv in January 2005, and it increased up to about 210 pptv by April 2012. This provides us with a rough estimate of the increase of HCFC-22 content: it had increased by 49 pptv in 7 years, which is roughly 7 pptv year^{-1}.

For a more detailed analysis, we consider the mean mixing ratios in 20° latitude bands (Figs. 13 and 14). In these figures, it is again visible that the zonal mean abundance of HCFC-22 over the equator is much higher than over the poles at similar altitudes. In addition to the latitude dependence of the absolute volume mixing ratios, the oscillations due to the seasonal cycle are more pronounced at higher latitudes for the stratosphere, while a pronounced seasonal cycle in the troposphere can also be found at 30–50° N. In the stratosphere at the poles, the break-up of the polar vortex, the latter being marked by low HCFC-22 abundances, results in a sharp increase of HCFC-22 in hemispheric spring. Interestingly, the break-up of the vortex seems to take place at all altitudes at almost the same time for the northern polar region, while for the southern polar regions a break-up starting at around 30 km and moving down, visible as higher HCFC-22 abundances occurring first around 30 km and low HCFC-22 abundances lasting longer at lower altitudes, can be observed. In this context it is also interesting to see that a local maximum of HCFC-22 appears just after vortex break-up around 30 km altitude (most pronounced in the years 2009 to 2011), which indicates that young HCFC-22-rich air from low latitudes is rapidly transported into the polar region at these altitudes. A similar observation has been made within the analysis of global distributions of mean age of stratospheric air (AoA) (Stiller et al., 2012). In mid-latitudes in the middle and upper stratosphere, there is no clear seasonal cycle visible, while at lower altitudes, in the so-called lowermost stratosphere (below 20 km), the maxima are shifted towards hemispheric late summer/fall. This is consistent with the current picture of the phases of the Brewer–Dobson circulation, where the extratropical lowermost stratosphere is thought to be flooded by young tropical air during summer

ACPD
15, 14783–14841, 2015

when the subtropical jet forms a weak mixing barrier only (Bönisch et al., 2011; Birner and Bönisch, 2011; Stiller et al., 2012).

Figure 15 provides the time series of HCFC-22 as latitude-time cross sections for certain altitude levels. At 10 and 14 km high seasonality in the northern subtropical latitudes with maxima during summer and caused by the Asian monsoon uplift is obvious. Around 20 km a clear seasonal cycle at high latitudes can be seen. Around 30 km, a QBO variation in the tropics modulates the seasonal variation, while at 44 km the pattern is dominated by the semi-annual oscillation.

Coming back to Fig. 12, it is obvious that the globally averaged distribution of HCFC-22 vmr in the stratosphere reveals also seasonal oscillations. This is due to the fact that SH seasonal cycle is not quite in the opposite phase to the cycle in the NH (see Fig. 15). In addition, the HCFC-22 seasonal cycle in the SH is more pronounced than in the NH, probably because of a more stable polar vortex which dominates the SH seasonal cycle. Hence, the seasonal cycle in the SH has a higher amplitude, and is not globally compensated but only weakened by the cycle of the NH. The hemispheric means of HCFC-22 vmr (Fig. 15) for the NH are generally higher than for the SH. This is due to higher industrial production of HCFC-22 in the NH.

5.3 Trend of HCFC-22

We have analysed time series of monthly means at specific altitudes for 10° wide latitude bands by fitting the following regression function to the data:

$$\mathrm{vmr}(t) = a + bt + c_1\,\mathrm{qbo}_1(t) + d_1\,\mathrm{qbo}_2(t) + \sum_{n=2}^{9}\left(c_n \sin\frac{2\pi t}{l_n} + d_n \cos\frac{2\pi t}{l_n}\right), \quad (1)$$

where t is time, qbo_1 and qbo_2 are QBO indices, and the terms under the sum are 8 sinusoidal functions of the period length l_n. The terms qbo_1 and qbo_2 are the normalized Singapore winds at 30 and 50 hPa as provided by the Free University of Berlin via http://www.geo.fu-berlin.de/met/ag/strat/produkte/qbo/index.html. qbo_1 and qbo_2 are

ACPD
15, 14783–14841, 2015

approximately orthogonal such that their combination can emulate any QBO phase shift (Kyrölä et al., 2010). Coefficients a, b, $c_1,\ldots,c_9$, $d_1,\ldots,d_9$ are fitted to the data using the method by von Clarmann et al. (2010), where the full error covariance matrix of the HCFC-22 data is considered, with the squared standard errors of the mean (SEM) of the monthly zonal means as the diagonal terms. Further, a constant model uncertainty error term has been added to the data error covariance matrix, which represents the deficiencies of the regression model with respect to the true atmospheric variation and was, within an iterative procedure, scaled such that the resulting χ^2_{reduced} of the trend fit was close to unity, corresponding to combined data and model uncertainties consistent to the fit residuals. Since we cannot exclude that these perturbations to be accounted for by this additional error term have a typical duration of more than one month, covariance terms between adjacent data points were also considered in order to account for the resulting autocorrelation. Phase shifts of the variations are represented by common use of sine and cosine functions of the same period length. The first and the second sinusoidal functions represent the seasonal and the semi-annual cycles, and have the periods of 12 and 6 months, respectively. In order to model the deviations of the temporal variation from pure sine or cosine shapes, i.e. to allow for irregular shapes like sawtooth shapes etc., the period lengths of the remaining 6 terms under the sum are chosen to be equal to 3, 4, 8, 9, 18 and 24 months. The general strategy of this particular fitting has been described in Stiller et al. (2012).

Figure 16 provides some examples for time series and their fits for 3 different latitude bins and two altitudes (40 to 50° S, 0 to 10° S, and 50 to 60° N, at 20 and 30 km, respectively). The lower panel of each figure provides the residuals between measured and fitted time series. The simple model is able to represent the observations very well in most cases. Besides the linear increase, for all altitude/latitude bins, a more or less pronounced seasonal cycle is the dominant feature of the time series. In the southern midlatitudes, a clear QBO signal is also present. For the northern midlatitudes at 30 km, we see also the impact of the semi-annual variation. The highest amplitudes in the temporal variation are reached in the 60° regions; in the inner tropics, the ampli-

ACPD
15, 14783–14841, 2015

tudes are lower, particularly in the lowermost stratosphere. A strong linear increase is present in all altitude/latitude bins and varies considerably.

Figure 17 summarises the derived decadal trends for all latitude/altitude bins. The trend is positive for all latitude and altitude bins and highly significant (significance of 5 σ or more). In the lowermost stratosphere below 20 km the trend is between 40 and 50 % decade^{-1}, while it varies between 30 % decade^{-1} in the northern middle and high latitudes between 20 and 30 km, 50 to 60 % decade^{-1} in the southern mid-latitudes from 20 to 50 km, and 70 to more than 100 % decade^{-1} in the northern upper stratosphere at middle and high latitudes.

Moore and Remedios (2008) have published growth rates of HCFC-22 in the lower stratosphere (approximately 20 km) between 20 and 50° N for the years 1994 to 2004 of 5.4 ± 0.7 pptv yr^{-1} (3.5 ± 0.4 % yr^{-1}); between 60 and 80° S they found 6.0 ± 0.7 pptv yr^{-1} (4.3 ± 0.5 % yr^{-1}) for the years 1994 to 2003. These values compare well to the growth rates found for the period 2005 to 2012 from MIPAS (see Figs. 16, left column, and 17). Rinsland et al. (2005a) published the following growth rates for lower stratospheric HCFC-22 vmrs near 30° N latitude from ATMOS/ACE-FTS measurements: in 1985 the rate was 14.57 ± 4.10 % yr^{-1}, in 1994 it was 6.35 ± 2.24 % yr^{-1}, and in 2004 it was 3.92 ± 2.08 % yr^{-1}. Our growth rate of 4 to 5 % yr^{-1} agrees reasonably well with the growth rate found for 2004.

The time series derived from Kitt Peak ground-based solar absorption measurements (Rinsland et al., 2005b) covers October 1987 to November 2002 with a best-fit increase rate of 5.66 ± 0.15 pptv yr^{-1} for the 2.09–10 km trend. Compared to this the tropospheric growth rate around 30° N derived from MIPAS for 2005 to 2012 is higher with a value around 7 pptv year^{-1}. Sherlock et al. (1997) derived exponential and linear increase rates of HCFC-22 between May 1985 and November 1994 at the station Lauder, New Zealand, of 7.5 ± 0.3 and 5.9 ± 0.2 % yr^{-1}. The growth rates derived from MIPAS for the lower stratosphere around 60° S are somewhat lower with 4 to 5 % yr^{-1}.

ACPD
15, 14783–14841, 2015

5.4 Comparisons with surface measurements of tropospheric growth rates

Two networks perform regular, long-term and highly precise measurements of various tracers, among them HCFC-22, close to the ground: these are the NOAA Earth System Research Laboratory (ESRL) Global Monitoring Division (GMD) and the Advanced Global Atmospheric Gases Experiment (AGAGE). Although not directly comparable, because MIPAS observations do not reach to the ground, we compare here mean tropospheric values (below 10 km altitude) retrieved from MIPAS data with the surface observations from NOAA/GMD and AGAGE, making use of the fact that the troposphere can be considered well-mixed. This assumption is confirmed by aircraft measurements (Xiang et al., 2014). In this context it should be noted that surface measurements are reported as dry air mole fraction, while stratospheric measurements are reported in mixing ratios where the air with its actual water vapour content is the reference. Since the stratosphere is very dry, this makes no discernable difference. Near surface, however, this difference has to be taken into account but since air dries during uplift, the surface dry air mole fraction is exactly the quantity which is comparable to our stratospheric values.

5.4.1 NOAA/GMD

NOAA/GMD runs flask measurements at remote site since 1992 (Montzka et al., 2009, 2014). These data are reported on the NOAA–2006 scale. Global HCFC-22 data from NOAA/GMD in units of mole fraction in dry air at ground level are shown in Fig. 18 for various measurement sites from the South Pole to the high Arctic. The data are not filtered for any pollution events, resulting in some enhanced values for the stations Trinidad Head and Mace Head that are occasionally influenced by nearby emissions. The MIPAS HCFC-22 monthly mean values for latitude bands selected to match the latitudes of the stations, averaged over all altitudes below 10 km, are shown for comparison with the same color code as the respective station data.

ACPD
15, 14783–14841, 2015

Overall NOAA data and MIPAS upper tropospheric values show a good agreement and similar trends. While according to MIPAS the HCFC-22 global mean below 10 km altitude (not shown) increased from 161 to 211 pptv between January 2005 and April 2012, the NOAA ground-based global mean for these months were 164 and 216 pptv, providing an increase of 50 (MIPAS) and 52 (NOAA) ppt, respectively. The growth rate derived from NOAA/GMD data for the NH is only slightly higher than that inferred from MIPAS measurements below 10 km (52 vs. 49 ppt over 7 years).

In the SH, tropospheric MIPAS values are mostly significantly higher than the NOAA values and reach the NOAA values only during their seasonal minima (Fig. 18). The reason is roughly this. MIPAS, whose measurements refer to the upper troposphere and above, sees more advected air from the tropical outflow, and the signal is modulated by a pronounced seasonal cycle, while the related ground-based measurements are clean-air measurements. This hypothesis is in tendency confirmed by SH aircraft measurements (e.g. Xiang et al., 2014), where an indication of higher mixing ratios at higher altitudes is found, which is attributed to transport of NH air into the SH at higher altitudes in lower latitudes. It is interesting to see that among the SH time series, the seasonal cycle in MIPAS data is strongest for the southern polar latitude band, while the minima reached within this time series are the lowest among all latitude bands. This strong seasonal cycle is also visible in Fig. 15 and indicates flooding of the southern polar UTLS region with low-latitude air around the time of the polar vortex breakdown.

The MIPAS measurements show smaller differences between the hemispheres than the NOAA measurements. This is explained by the fact that MIPAS observes air at altitudes where the outflow of the tropical pipe contributes to the composition of air. Assuming that air uplifted within the tropical pipe is mixed between both hemispheres offers an explanation for the reduced hemispheric contrast in the MIPAS data. Also these findings are in agreement with those of Xiang et al. (2014).

Finally, the most obvious difference between NOAA/GMD surface time series and zonally averaged MIPAS upper troposphere time series is the pronounced seasonal cycle in the latter, with minimum values during NH spring and SH summer. Xiang et al.

ACPD
15, 14783–14841, 2015

(2014) observed a seasonality in NOAA surface measurements of HCFC-22 with minima in northern summer and attributed this to increased scavenging through the OH radical reaction and seasonality in the transport. The best explanation of the observed seasonality, however, relies on an additional seasonality of the emissions of refrigerants with maxima in summer. This seasonality of emissions was derived by inverse modelling of aircraft measurements (Xiang et al., 2014). While OH scavenging and seasonal variations in transport could possibly explain the summer minimum observed by MIPAS in the SH, the springtime minimum in the NH is more probably related to intrusion of HCFC-22-poor stratospheric air at the end of the polar winter and during polar vortex breakdown. Similar springtime minima were also observed for other tropospheric source gases and have been attributed to stratospheric air intrusions (Nevison et al., 2004, 2011). The fact that the minima in the MIPAS time series at higher altitudes precede those at lower altitudes (cf. Fig. 14, lowermost panel, and Fig. 15) supports this. The amplitude of the seasonal cycle seems to be even more enhanced due to transport of high HCFC-22 abundances uplifted within the Asian monsoon anticyclone to higher latitudes during fall (compare Fig. 15, top panel).

5.4.2 AGAGE

AGAGE provides in situ measurements of a wide range of ozone depleting compounds and greenhouse gases, including HCFC-22, from several ground stations (Prinn et al., 2000, 2013; O'Doherty et al., 2004). AGAGE measurements used here are obtained using in situ gas chromatography with mass spectrometry (GC-MS) detection technique and are reported on the SIO-2005 calibration scale. NOAA flask results and AGAGE in situ data are compared every six months at common sites. Comparison of HCFC-22 from NOAA flasks, using the NOAA–2006 calibration scale to AGAGE in situ measurements based on the SIO-05 calibration scale at Cape Grim, Samoa, Trinidad Head and Mace Head reveal the following differences: the average difference (NOAA minus AGAGE) across the 4 sites is -0.7 ± 0.5 ppt or 0.35 ± 0.25 %. The differences are

ACPD
15, 14783–14841, 2015

also relatively constant with time. These results are also very consistent to those found in the International Halocarbons in Air Comparison Experiment (Hall et al., 2014).

Figure 19 shows the HCFC-22 time series of these stations, which represent various latitude bands from northern to southern mid-latitudes. The variation among the values from different stations represent the inter-hemispheric differences of HCFC-22: NH values are about 10 % higher than SH values, due to the main sources of HCFC-22 being located in the NH. Again, we have inserted for comparison MIPAS HCFC-22 global monthly mean values averaged for all altitudes below 10 km. The MIPAS data generally agree well with the tropical time series from the AGAGE network, both in absolute values and in the growth rate. As already seen in the NOAA comparison, the seasonal cycle in MIPAS data in the NH is far more pronounced and its amplitude increases towards high latitudes. Maximum values fit perfectly to AGAGE station data in the NH. The same explanation applies that was offered in the previous section: Arctic winter subsidence of HCFC-22-poor stratospheric air modulates the upper tropospheric NH time series with a northern winter/spring minimum.

The SH upper tropospheric annual cycle is not exactly in the opposite phase of its northern counterpart. The latitudes of the SH stations shown in this comparison are, however, generally lower than the latitudes of the NH stations. At these low latitudes the upper tropospheric air is not modulated that much by polar processes but by the change of the position of the inner-tropical convergence zone and the Hadley cell. In local summer these latitudes are affected by the outflow of the tropical pipe, providing young HCFC-22-rich air. This hypothesis is corroborated by the fact that the MIPAS time series at 45–35° S (pink full circles in Fig. 19) follows nicely the Cape Matatula (Samoa) (13° S, blue open squares) time series, while it appears to be uncorrelated with the Cape Grim (Tasmania) (42° S) data.

5.5 Unexplained stratospheric trends

Differences between the MIPAS stratospheric percentage trends (relative to the HCFC-22 vmr in 2005) and the tropospheric trends corrected for AoA from NOAA/GMD are

ACPD
15, 14783–14841, 2015

shown in Fig. 20. We used the NOAA/GMD global trends, extended linearly with a slope of 57 ppt decade^{-1} before 1992, and AoA from Stiller et al. (2012), according to the method described in Kellmann et al. (2012). We would like to stress that we do not necessarily expect the stratospheric trends to reproduce the tropospheric ones with a time lag depending on the AoA, because stratospheric circulation could change, affecting the time lag and possibly the level of HCFC-22 change in the air parcel observed. Furthermore the AoA spectrum could, in the case of a non-linearly increasing species, render the mean AoA non-representative. However, for an atmosphere without changes in stratospheric dynamics and δ-shaped age spectra, the differences shown in Fig. 20 are expected to be zero throughout. In contrast, we find positive and negative trend differences of up to 40 % . The HCFC-22 trend in the northern mid-latitude lower stratosphere (15–30 km) is slightly smaller (up to −10 %) than the trend at the ground at the time the air started its travel into the stratosphere, while in the southern midlatitudes, the HCFC-22 trend is larger than the trend observed at surface level over all the stratosphere. In the polar regions, the trend is up to 40 % lower at the South pole, and up to 40 % higher at the North pole and the northern mid-latitudes. This pattern of trend differences is in agreement with the patterns found for CFC-11 and CFC-12 (Kellmann et al., 2012), and is in accordance with the AoA trends found by Stiller et al. (2012). Positive AoA trends in the northern midlatitudes below 30 km and the southern polar region lead to increasingly longer exposure of HCFC-22 to loss processes in the stratosphere, and thus to a reduction of the positive HCFC-22 trend, while the general positive HCFC-22 trend is further increased in regions where the AoA becomes younger, leaving less time for stratospheric HCFC-22 loss processes. It should be noted that any incorrect assumption on AoA as such, used within the correction of surface trends, cannot explain both the positive and negative signs in the trend differences. The surface trend was slightly increasing all over the observation period covered by NOAA/GMD measurements, thus the correction by the AoA should always lead to smaller trends. Any incorrect assumption on the AoA would lead to incorrect differences, which, however, had always the same positive or negative sign. Thus, the

ACPD
15, 14783–14841, 2015

occurrence of positive and negative trend differences is an unambiguous sign that the circulation must have changed over the MIPAS observation period. Our results further show that these circulation changes were different in the northern and southern midlatitudes, as was concluded from the AoA data inferred from the MIPAS SF_6 data record (Stiller et al., 2012).

6 Summary and conclusions

HCFC-22 data from MIPAS for the period 2005 to 2012 were produced and analyzed. Version 5 level-1b reduced resolution MIPAS measurements (nominal mode) of the period from 27 January 2005 to 8 April 2012 were inverted using the MIPAS IMK/IAA scientific data processor. The profile retrieval was performed by Tikhonov-constrained non-linear least squares fitting of measured limb spectral radiances. The total error of the retrieval is 7 % on 20 km height and 9 % on 30 km height, and the error budget is dominated by noise. A typical retrieved profile represents approximately 5° of freedom, corresponding to an altitude resolution of typically between 3 km at 10 km height and 7 km at 30 km height, further increasing with height. The percentage of non-converged profiles is about 0.01 to 0.02 %.

The obtained profiles were compared with ACE-FTS satellite data (v3.5), as well as with MkIV balloon profiles and in situ measurements performed by the University of Frankfurt. The comparisons are ambiguous with respect to a bias of MIPAS measurements; in general we can state that MIPAS agrees within ±15 pptv (1-σ) with ACE-FTS and MkIV the reference measurements. Between 13 and 22 km, good agreement with MkIV and ACE-FTS profiles is demonstrated. A high bias of 30–50 pptv relative to cryosampler measurements was found below 24 km but no bias was found for higher altitudes.

The global distribution of HCFC-22 vmr reflects the mean circulation in the stratosphere and reveals also seasonal oscillations. The HCFC-22 annual cycle in the SH is more pronounced than in the NH. The HCFC-22 volume mixing ratio in the NH tro-

ACPD
15, 14783–14841, 2015

posphere is generally higher than in the SH, due to main emission sources residing there. A volume mixing ratio maximum is situated at about 16 km height at low latitudes, which exceeds mixing ratios measured at all remote surface sites an in the NH or SH. We attribute this to advection to low latitudes of HCFC-22-rich air uplifted in the Asian monsoon area. The source of this HCFC-22-rich air could be South-East Asia. United Nations Environment Programme (2012) reports that China has been the largest global producer and consumer of HCFCs for a number of years.

A multi-variate regression analysis was performed for 10° latitude/1–2 km altitude bins, with terms for linear variations, sinusoidal variations with various periods, and a proxy for the QBO variation. We find positive linear trends for all latitude/altitude bins, ranging from 83 pptv decade^{-1} in the northern subtropical lower stratosphere to 18 pptv decade^{-1} in the southern polar upper stratosphere. The percentage trends agree well with previous analyses. Percentage trends are highest in the southern mid-latitudinal stratosphere (50–70 % decade^{-1}) and in the northern polar upper stratosphere (70 to 120 % decade^{-1}) and lowest in the northern lowermost stratosphere (around 30 % decade^{-1}). The highest seasonal amplitudes are observed in the 60° regions; in the tropical lower stratosphere the amplitudes are low.

Global NOAA/GMD, AGAGE and MIPAS tropospheric values show good absolute agreement and similar trends. Based on the absolute values of HCFC-22 from MIPAS and on the MIPAS derived HCFC-22-growth rate, one can conclude that the HCFC-22 global volume mixing ratio in the lower stratosphere has risen by 49 pptv in 7 years. A pronounced seasonality has been detected in the upper troposphere with minima in spring in the NH and in local summer in the SH. The latter is attributed to the seasonality of the main tropical uplift and outflow regions. The seasonality in the NH is attributed to the intrusion of HCFC-22-poor stratospheric air at the end of the Arctic winter. Inconsistencies in percentage trends between ground-based and age-corrected MIPAS stratospheric trends hint at recent changes in stratospheric circulation. Similar indication has been found by analysis of trends of the mean AoA (Stiller et al., 2012), ozone

ACPD
15, 14783–14841, 2015

(Eckert et al., 2014) and CFC-11 as well as CFC-12 (Kellmann et al., 2012). A more detailed analysis of these circulation changes is currently under investigation.

Acknowledgements. We acknowledge provision of MIPAS level-1b data by ESA. NOAA measurements of HCFC-22 are made possible in part by funding from the NOAA Climate Program Office's AC4 program. Standards, flask handling, and flask analysis at NOAA are provided with assistance from B. Hall, C. Siso, and D. Mondeel. AGAGE is supported principally by NASA (USA) grants to MIT and SIO, and also by: DECC (UK) and NOAA (USA) grants to Bristol University; CSIRO and the Bureau of Meteorology (Australia); FOEN grants to Empa (Switzerland); NILU (Norway); SNU (Korea); CMA (China); NIES (Japan); and Urbino University (Italy). Part of this research was performed at the Jet Propulsion Laboratory, California Institute of Technology, under contract with NASA. We thank the Columbia Scientific Balloon Facility (CSBF) for performing the launches of the JPL MkIV instrument. The Atmospheric Chemistry Experiment (ACE), also known as SCISAT, is a Canadian-led mission mainly supported by the Canadian Space Agency and the Natural Sciences and Engineering Research Council of Canada. Data analysis at IMK has been supported by BmBF under contract number 50EE0901.

The article processing charges for this open-access publication were covered by a Research Centre of the Helmholtz Association.

References

Bernath, P. F., McElroy, C. T., Abrams, M. C., Boone, C. D., Butler, M., Camy-Peyret, C., Carleer, M., Clerbaux, C., Coheur, P.-F., Colin, R., DeCola, P., De Mazière, M., Drummond, J. R., Dufour, D., Evans, W. F. J., Fast, H., Fussen, D., Gilbert, K., Jennings, D. E., Llewellyn, E. J., Lowe, R. P., Mahieu, E., McConnell, J. C., McHugh, M., McLeod, S. D., Michaud, R., Midwinter, C., Nassar, R., Nichitiu, F., Nowlan, C., Rinsland, C. P., Rochon, Y. J., Rowlands, N., Semeniuk, K., Simon, P., Skelton, R., Sloan, J. J., Soucy, M.-A., Strong, K., Tremblay, P., Turnbull, D., Walker, K. A., Walkty, I., Wardle, D. A., Wehrle, V., Zander, R., and Zou, J.: Atmospheric Chemistry Experiment (ACE): mission overview, Geophys. Res. Lett., 32, L15S01, doi:10.1029/2005GL022386, 2005. 14792

ACPD
15, 14783–14841, 2015

Birner, T. and Bönisch, H.: Residual circulation trajectories and transit times into the extratropical lowermost stratosphere, Atmos. Chem. Phys., 11, 817–827, doi:10.5194/acp-11-817-2011, 2011. 14801

Bönisch, H., Engel, A., Birner, Th., Hoor, P., Tarasick, D. W., and Ray, E. A.: On the structural changes in the Brewer-Dobson circulation after 2000, Atmos. Chem. Phys., 11, 3937–3948, doi:10.5194/acp-11-3937-2011, 2011. 14801

Boone, C. D., Nassar, R., Walker, K. A., Rochon, Y., McLeod, S. D., Rinsland, C. P., and Bernath, P. F.: Retrievals for the atmospheric chemistry experiment Fourier–transform spectrometer, Appl. Optics, 44, 7218–7231, 2005. 14792

Boone, C. D., Walker, K. A., and Bernath, P. F.: Version 3 retrievals for the Atmospheric Chemistry Experiment Fourier Transform Spectrometer (ACE-FTS), in: The Atmospheric Chemistry Experiment ACE at 10: a Solar Occultation Anthology, edited by: Bernath, P. F., A. Deepak Publishing, Hampton, Virginia, USA, 103–127, 2013. 14792

Carlotti, M.: Global–fit approach to the analysis of limb–scanning atmospheric measurements, Appl. Optics, 27, 3250–3254, 1988. 14789

Eckert, E., von Clarmann, T., Kiefer, M., Stiller, G. P., Lossow, S., Glatthor, N., Degenstein, D. A., Froidevaux, L., Godin-Beekmann, S., Leblanc, T., McDermid, S., Pastel, M., Steinbrecht, W., Swart, D. P. J., Walker, K. A., and Bernath, P. F.: Drift-corrected trends and periodic variations in MIPAS IMK/IAA ozone measurements, Atmos. Chem. Phys., 14, 2571–2589, doi:10.5194/acp-14-2571-2014, 2014. 14811

Endemann, M. and Fischer, H.: Envisat's High–Resolution Limb Sounder: MIPAS, ESA Bull.-Eur. Space, 76, 47–52, 1993. 14787

Endemann, M., Gare, P., Smith, D., Hoerning, K., Fladt, B., and Gessner, R.: MIPAS Design Overview and Current Development Status, in: Proceedings EUROPTO Series, Optics in Atmospheric Propagation, Adaptive Systems, and Lidar Techniques for Remote Sensing, Taormina, Italy, 24–26 September 1996, vol. 2956, 124–135, 1996. 14787

Engel, A., Schmidt, U., and Stachnik, R. A.: Partitioning between chlorine reservoir species deduced from observations in the Arctic winter stratosphere, J. Atmos. Chem., 27, 107–126, 1997. 14786, 14794

European Space Agency: Envisat, MIPAS An Instrument for Atmospheric Chemistry and Climate Research, ESA Publications Division, ESTEC, P.O. Box 299, 2200 AG Noordwijk, the Netherlands, SP-1229, 2000. 14787

ACPD
15, 14783–14841, 2015

Fischer, H. and Oelhaf, H.: Remote sensing of vertical profiles of atmospheric trace constituents with MIPAS limb-emission spectrometers, Appl. Optics, 35, 2787–2796, 1996. 14787

Fischer, H., Birk, M., Blom, C., Carli, B., Carlotti, M., von Clarmann, T., Delbouille, L., Dudhia, A., Ehhalt, D., Endemann, M., Flaud, J. M., Gessner, R., Kleinert, A., Koopman, R., Langen, J., López-Puertas, M., Mosner, P., Nett, H., Oelhaf, H., Perron, G., Remedios, J., Ridolfi, M., Stiller, G., and Zander, R.: MIPAS: an instrument for atmospheric and climate research, Atmos. Chem. Phys., 8, 2151–2188, doi:10.5194/acp-8-2151-2008, 2008. 14788

Gardiner, T., Forbes, A., de Mazière, M., Vigouroux, C., Mahieu, E., Demoulin, P., Velazco, V., Notholt, J., Blumenstock, T., Hase, F., Kramer, I., Sussmann, R., Stremme, W., Mellqvist, J., Strandberg, A., Ellingsen, K., and Gauss, M.: Trend analysis of greenhouse gases over Europe measured by a network of ground-based remote FTIR instruments, Atmos. Chem. Phys., 8, 6719–6727, doi:10.5194/acp-8-6719-2008, 2008. 14787

Goldman, A., Murcray, F. J., Blatherwick, R. D., Bonomo, F. S., Murcray, F. H., and Murcray, D. G.: Spectroscopic identification of $CHClF_2$ (F-22) in the lower stratosphere, Geophys. Res. Lett., 8, 1012–1014, doi:10.1029/GL008i009p01012, 1981. 14787

Hall, B. D., Engel, A., Mühle, J., Elkins, J. W., Artuso, F., Atlas, E., Aydin, M., Blake, D., Brunke, E.-G., Chiavarini, S., Fraser, P. J., Happell, J., Krummel, P. B., Levin, I., Loewenstein, M., Maione, M., Montzka, S. A., O'Doherty, S., Reimann, S., Rhoderick, G., Saltzman, E. S., Scheel, H. E., Steele, L. P., Vollmer, M. K., Weiss, R. F., Worthy, D., and Yokouchi, Y.: Results from the International Halocarbons in Air Comparison Experiment (IHALACE), Atmos. Meas. Tech., 7, 469–490, doi:10.5194/amt-7-469-2014, 2014. 14794, 14807

Hoyle, C. R., Marécal, V., Russo, M. R., Allen, G., Arteta, J., Chemel, C., Chipperfield, M. P., D'Amato, F., Dessens, O., Feng, W., Hamilton, J. F., Harris, N. R. P., Hosking, J. S., Lewis, A. C., Morgenstern, O., Peter, T., Pyle, J. A., Reddmann, T., Richards, N. A. D., Telford, P. J., Tian, W., Viciani, S., Volz-Thomas, A., Wild, O., Yang, X., and Zeng, G.: Representation of tropical deep convection in atmospheric models – Part 2: Tracer transport, Atmos. Chem. Phys., 11, 8103–8131, doi:10.5194/acp-11-8103-2011, 2011. 14799

Kellmann, S., von Clarmann, T., Stiller, G. P., Eckert, E., Glatthor, N., Höpfner, M., Kiefer, M., Orphal, J., Funke, B., Grabowski, U., Linden, A., Dutton, G. S., and Elkins, J. W.: Global CFC-11 (CCl_3F) and CFC-12 (CCl_2F_2) measurements with the Michelson Interferometer for Passive Atmospheric Sounding (MIPAS): retrieval, climatologies and trends, Atmos. Chem. Phys., 12, 11857–11875, doi:10.5194/acp-12-11857-2012, 2012. 14808, 14811

ACPD
15, 14783–14841, 2015

Kiefer, M., von Clarmann, T., and Grabowski, U.: State parameter data base for MIPAS data analysis, Adv. Space Res., 30, 2387–2392, 2002. 14789

Kiefer, M., Arnone, E., Dudhia, A., Carlotti, M., Castelli, E., von Clarmann, T., Dinelli, B. M., Kleinert, A., Linden, A., Milz, M., Papandrea, E., and Stiller, G.: Impact of temperature field inhomogeneities on the retrieval of atmospheric species from MIPAS IR limb emission spectra, Atmos. Meas. Tech., 3, 1487–1507, doi:10.5194/amt-3-1487-2010, 2010. 14789

Kolonjari, F., Walker, K. A., Boone, C. D., Strahan, S., McLinden, C. A., Manney, G. L., Daffer, W. H., and Bernath, P. F.: ACE-FTS measurements of HCFC-22, Geophys. Res. Abstracts, 14, EGU2012-12440, 2012. 14787

Kyrölä, E., Tamminen, J., Sofieva, V., Bertaux, J. L., Hauchecorne, A., Dalaudier, F., Fussen, D., Vanhellemont, F., Fanton d'Andon, O., Barrot, G., Guirlet, M., Fehr, T., and Saavedra de Miguel, L.: GOMOS O_3, NO_2, and NO_3 observations in 2002–2008, Atmos. Chem. Phys., 10, 7723–7738, doi:10.5194/acp-10-7723-2010, 2010. 14802

Laube, J. C., Engel, A., Bönisch, H., Möbius, T., Worton, D. R., Sturges, W. T., Grunow, K., and Schmidt, U.: Contribution of very short-lived organic substances to stratospheric chlorine and bromine in the tropics – a case study, Atmos. Chem. Phys., 8, 7325–7334, doi:10.5194/acp-8-7325-2008, 2008. 14794

Montzka, S. A., Butler, J. H., Hall, B., Mondeel, D., and Elkins, J. W.: A decline in tropospheric organic bromine, Geophys. Res. Lett., 30, 1826, doi:10.1029/2003GL017745, 2003. 14794

Montzka, S. A., Hall, B. D., and Elkins, J. W.: Accelerated increases observed for Hydrochlorofluorocarbons since 2004 in the global atmosphere, Geophys. Res. Lett., 36, L03804, doi:10.1029/2008GL036475, 2009. 14786, 14799, 14804

Montzka, S. A., McFarland, M., Andersen, S. O., Miller, B. R., Fahey, D. W., Hall, B. D., Hu, L., Siso, C., and Elkins, J. W.: Recent Trends in Global Emissions of Hydrochlorofluorocarbons and Hydrofluorocarbons: Reflecting on the 2007 Adjustments to the Montreal Protocol, J. Phys. Chem. A, 119, 4439–4449, doi:10.1021/jp5097376, 2014. 14804

Moore, D. P. and Remedios, J. J.: Growth rates of stratospheric HCFC-22, Atmos. Chem. Phys., 8, 73–82, doi:10.5194/acp-8-73-2008, 2008. 14786, 14787, 14803

Murcray, D. G., Bonomo, F. S., Brooks, J. N., Goldman, A., Murcray, F. H., and Williams, W. J.: Detection of fluorocarbons in the stratosphere, Geophys. Res. Lett., 2, 109–112, 1975. 14787

Nett, H., Carli, B., Carlotti, M., Dudhia, A., Fischer, H., Flaud, J.-M., Perron, G., Raspollini, P., and Ridolfi, M.: MIPAS Ground Processor and Data Products, in: Proc. IEEE 1999 Inter-

ACPD
15, 14783–14841, 2015

national Geoscience and Remote Sensing Symposium, 28 June–2 July 1999, Hamburg, Germany, 1692–1696, 1999. 14788

Nevison, C. D., Kinnison, D. E., and Weiss, R. F.: Stratospheric influences on the tropospheric seasonal cycles of nitrous oxide and chlorofluorocarbons, Geophys. Res. Lett., 31, L20103, doi:10.1029/2004GL020398, 2004. 14806

Ofner, J., Krüger, H.-U., Grothe, H., Schmitt-Kopplin, P., Whitmore, K., and Zetzsch, C.: Physico-chemical characterization of SOA derived from catechol and guaiacol – a model substance for the aromatic fraction of atmospheric HULIS, Atmos. Chem. Phys., 11, 1–15, doi:10.5194/acp-11-1-2011, 2011. 14806

Norton, H. and Beer, R.: New apodizing functions for Fourier spectrometry, J. Opt. Soc. Am., 66, 259–264, (Errata J. Opt. Soc. Am., 67, 419, 1977), 1976. 14788

O'Doherty, S., Cunnold, D. M., Manning, A., Miller, B. R., Wang, R. H. J., Krummel, P. B., Fraser, P. J., Simmonds, P. G., McCulloch, A., Weiss, R. F., Salameh, P., Porter, L. W., Prinn, R. G., Huang, J., Sturrock, G., Ryall, D., Derwent, R. G., and Montzka, S. A.: Rapid growth of hydrofluorocarbon 134a and hydrochlorofluorocarbons 141b, 142b, and 22 from Advanced Global Atmospheric Gases Experiment (AGAGE) observations at Cape Grim, Tasmania, and Mace Head, Ireland, J. Geophys. Res., 109, D06310, doi:10.1029/2003JD004277, 2004. 14786, 14806

Park, M., Randel, W. J., Kinnison, D. E., Bernath, P. F., Walker, K. A., Boone, C. D., Atlas, E. L., Montzka, S. A., and Wofsy, S. C.: Global Trends of $CHClF_2$ (HCFC-22) and CCl_3F (CFC-11) estimated from ACE-FTS, HIPPO and WACCM4, in: SPARC General Assembly 2014, 12–17 January 2014, Queenstown, NZ, 2014. 14787

Ploeger, F., Konopka, P., Müller, R., Fueglistaler, S., Schmidt, T., Manners, J. C., Grooß, J.-U., Günther, G., Forster, P. M., and Riese, M.: Horizontal transport affecting trace gas seasonality in the Tropical Tropopause Layer (TTL), J. Geophys. Res., 117, D09303, doi:10.1029/2011JD017267, 2012. 14799

Prinn, R. G., Weiss, R. F., Fraser, P. J., Simmonds, P. G., Cunnold, D. M., Alyea, F. N., O'Doherty, S., Salameh, P., Miller, B. R., Huang, J., Wang, R. H. J., Hartley, D. E., Harth, C., Steele, L. P., Sturrock, G., Midgley, P. M., and McCulloch, A.: A history of chemically and radiatively important gases in air deduced from ALE/GAGE/AGAGE, J. Geophys. Res., 105, 17,751–17,792, doi:10.1029/2000JD900141, 2000. 14806

Prinn, R. G., Weiss, R. F., Fraser, P. J., Simmonds, P. G., Cunnold, D. M., O'Doherty, S., Salameh, P. K., Porter, L. W., Krummel, P. B., Wang, R. H. J., Miller, B. R., Harth, C., Gre-

ACPD
15, 14783–14841, 2015

ally, B. R., Van Woy, F. A., Steele, L. P., Mühle, J., Sturrock, G. A., Alyea, F. N., Huang, J., and Hartley, D. E.: The ALE/GAGE AGAGE Network, Carbon Dioxide Information Analysis Center (CDIAC), Oak Ridge National Laboratory (ORNL), US Department of Energy (DOE), 2013. 14806

Randel, W. J. and Jensen, E. J.: Physical processes in the tropical tropopause layer and their role in a changing climate, Nat. Geosci., 6, 169–176, doi:10.1038/ngeo1733, 2013. 14799

Rasmussen, R. A., Khalil, M. A. K., Penkett, S. A., and Prosser, N. J. D.: $CHClF_2$ (F-22) in the Earth's atmosphere, Geophys. Res. Lett., 7, 809–812, doi:10.1029/GL007i010p00809, 1980. 14786

Rinsland, C. P., Boone, C., Nassar, R., Walker, K., Bernath, P., Mahieu, E., Zander, R., McConnell, J. C., and Chiou, L.: Trends of HF, HCl, CCl_2F_2, CCl_3F, $CHCLF_2$ (HCFC-22), and SF_6 in the lower stratosphere from Atmospheric Chemistry Experiment (ACE) and Atmospheric Trace Molecule Spectroscopy (ATMOS) measurements near 30° N latitude, Geophys. Res. Lett., 32, L16S03, doi:10.1029/2005GL022415, 2005a. 14787, 14803

Rinsland, C. P., Chiou, L. S., Goldman, A., and Wood, S. W.: Long-term trend in CHF_2Cl (HCFC-22) from high spectral resolution infrared solar absorption measurements and comparison with in situ measurements, J. Quant. Spectrosc. Ra., 90, 367–375, doi:10.1016/j.jqsrt.2004.04.008, 2005b. 14787, 14803

Rodgers, C. D.: Inverse Methods for Atmospheric Sounding: Theory and Practice, vol. 2 of Series on Atmospheric, Oceanic and Planetary Physics, edited by: Taylor, F. W., World Scientific, Singapore, New Jersey, London, Hong Kong, 2000. 14790

Saikawa, E., Rigby, M., Prinn, R. G., Montzka, S. A., Miller, B. R., Kuijpers, L. J. M., Fraser, P. J. B., Vollmer, M. K., Saito, T., Yokouchi, Y., Harth, C. M., Mühle, J., Weiss, R. F., Salameh, P. K., Kim, J., Li, S., Park, S., Kim, K.-R., Young, D., O'Doherty, S., Simmonds, P. G., McCulloch, A., Krummel, P. B., Steele, L. P., Lunder, C., Hermansen, O., Maione, M., Arduini, J., Yao, B., Zhou, L. X., Wang, H. J., Elkins, J. W., and Hall, B.: Global and regional emission estimates for HCFC-22, Atmos. Chem. Phys., 12, 10033–10050, doi:10.5194/acp-12-10033-2012, 2012. 14798

Sherlock, V. J., Jones, N. B., Matthews, W. A., Murcray, F. J., Blatherwick, R. D., Murcray, D. G., Goldman, A., Rinsland, C. P., Bernardo, C., and Griffith, D. W. T.: Increase in the vertical column abundance of HCFC-22 ($CHClF_2$) above Lauder, New Zealand, between 1985 and 1994, J. Geophys. Res., 102, 8861–8865, doi:10.1029/96JD01012, 1997. 14803

ACPD
15, 14783–14841, 2015

Steck, T.: Methods for determining regularization for atmospheric retrieval problems, Appl. Optics, 41, 1788–1797, 2002. 14791
Stiller, G. P. (Ed.): The Karlsruhe Optimized and Precise Radiative Transfer Algorithm (KOPRA), vol. FZKA 6487 of Wissenschaftliche Berichte, Forschungszentrum Karlsruhe, Karlsruhe, 2000. 14789
Stiller, G. P., von Clarmann, T., Haenel, F., Funke, B., Glatthor, N., Grabowski, U., Kellmann, S., Kiefer, M., Linden, A., Lossow, S., and López-Puertas, M.: Observed temporal evolution of global mean age of stratospheric air for the 2002 to 2010 period, Atmos. Chem. Phys., 12, 3311–3331, doi:10.5194/acp-12-3311-2012, 2012. 14800, 14801, 14802, 14808, 14809, 14810
Tikhonov, A.: On the solution of incorrectly stated problems and method of regularization, Dokl. Akad. Nauk. SSSR+, 151, 501–504, 1963. 14789
Toon, G. C.: The JPL MkIV Interferometer, Opt. Photonics News, 2, 19–21, 1991. 14796
United Nations Environment Programme: Handbook for the Montreal Protocol on Substances that Deplete the Ozone Layer, Eighth edition, Nairobi, Kenya, 2009. 14786
United Nations Environment Programme: Handbook for the Montreal Protocol on Substances that Deplete the Ozone Layer, Ninth edition, Nairobi, Kenya, 2012. 14810
von Clarmann, T.: Validation of remotely sensed profiles of atmospheric state variables: strategies and terminology, Atmos. Chem. Phys., 6, 4311–4320, doi:10.5194/acp-6-4311-2006, 2006. 14793
von Clarmann, T.: Chlorine in the stratosphere, Atmósfera, 26, 415–458, 2013. 14787
von Clarmann, T., Glatthor, N., Grabowski, U., Höpfner, M., Kellmann, S., Kiefer, M., Linden, A., Mengistu Tsidu, G., Milz, M., Steck, T., Stiller, G. P., Wang, D. Y., Fischer, H., Funke, B., Gil-López, S., and López-Puertas, M.: Retrieval of temperature and tangent altitude pointing from limb emission spectra recorded from space by the Michelson Interferometer for Passive Atmospheric Sounding (MIPAS), J. Geophys. Res., 108, 4736, doi:10.1029/2003JD003602, 2003. 14789
von Clarmann, T., De Clercq, C., Ridolfi, M., Höpfner, M., and Lambert, J.-C.: The horizontal resolution of MIPAS, Atmos. Meas. Tech., 2, 47–54, doi:10.5194/amt-2-47-2009, 2009. 14791, 14820
von Clarmann, T., Stiller, G., Grabowski, U., Eckert, E., and Orphal, J.: Technical Note: Trend estimation from irregularly sampled, correlated data, Atmos. Chem. Phys., 10, 6737–6747, doi:10.5194/acp-10-6737-2010, 2010. 14802

ACPD
15, 14783–14841, 2015

Williams, W. J., Kosters, J. J., Goldman, A., and Murcray, D. G.: Measurements of stratospheric halocarbon distributions using infrared techniques, Geophys. Res. Lett., 3, 379–382, doi:10.1029/GL003i007p00379, 1976. 14787

World Meteorological Organization (WMO): Scientific Assessment of Ozone Depletion: 2014, Global Ozone Research and Monitoring Project – Report No. 55, 416 pp., Geneva, Switzerland, 2014. 14786

Xiang, B., Patra, P. K., Montzka, S. A., Miller, S. M., Elkins, J. W., Moore, F. L., Atlas, A. L., Miller, B. R., Weiss, R. F., Prinn, R. G., and Wofsy, S. C.: Global emissions of refrigerants HCFC-22 and HCFC-134a: unforeseen seasonal contributions, P. Natl. Acad. Sci. USA, 111, 17379–17384, doi:10.1073/pnas.1417372111, 2014. 14792, 14798, 14804, 14805, 14806

Yokouchi, Y., Taguchi, S., Saito, T., Tohjima, Y., Tanimoto, H., and Mukai, H.: High frequency measurements of HFCs at a remote site in east Asia and their implications for Chinese emissions, Geophys. Res. Lett., 33, L21814, doi:10.1029/2006GL026403, 2006. 14786

Zander, R., Rinsland, C. P., Farmer, C. B., and Norton, R. H.: Infrared spectroscopic measurements of halogenated source gases in the stratosphere with the ATMOS instrument, J. Geophys. Res., 92, 9836–9850, 1987. 14787

Zander, R., Mahieu, E., Demoulin, P., Duchatelet, P., Servais, C., Roland, G., Delbouille, L., Mazière, M. D., and Rinsland, C. P.: Evolution of a dozen non-CO_2 greenhouse gases above central Europe since the mid-1980s, Environ. Sci., 2, 295–303, doi:10.1080/15693430500397152, 2005. 14787

ACPD
15, 14783–14841, 2015

Table 1. Error budget of a V5r HCFC-22 (nominal mode, reduced resolution) retrieval on 9 January 2009, 18.6° S latitude and 111.6° W longitude, orbit 35874, for selected altitudes. The errors are given in units of mixing ratios (pptv), and additionally, in parentheses, in percentage units (%).

V5r HCFC-22 Height	Total Error	Noise	Parameter Error	O_3	LOS	Shift	Gain	ILS
40 km	14 (17.3)	13 (16.1)	5.7 (7.0)	0.3 (0.3)	1.7 (2.1)	1.9 (2.3)	0.3 (0.3)	2.3 (2.8)
35 km	12 (11.2)	11 (10.2)	6.1 (5.7)	0.2 (0.1)	1.4 (1.3)	2.3 (2.1)	0.5 (0.5)	1.5 (1.4)
30 km	12 (9.0)	9.4 (7.1)	7.3 (5.5)	< 0.1 (< 0.1)	1.1 (0.8)	2.3 (1.7)	1.0 (0.7)	0.4 (0.3)
25 km	13 (8.0)	9.0 (5.6)	9.1 (5.6)	0.2 (0.1)	3.2 (2.0)	1.2 (0.7)	0.6 (0.3)	0.8 (0.5)
20 km	14 (7.0)	8.2 (4.1)	12 (6.0)	0.3 (0.2)	5.2 (2.6)	0.5 (0.2)	0.5 (0.2)	2.4 (1.2)
15 km	13 (5.6)	7.1 (3.1)	11 (4.7)	0.3 (0.1)	1.2 (0.5)	0.8 (0.3)	1.6 (0.7)	2.8 (1.2)
10 km	13 (6.8)	8.6 (4.5)	9.6 (5.0)	< 0.1 (< 0.1)	1.8 (0.9)	0.1 (< 0.1)	2.1 (1.1)	2.0 (1.0)

ACPD
15, 14783–14841, 2015

Table 2. Horizontal averaging kernels (full width at half maximum) calculated according to von Clarmann et al. (2009) for retrieval altitudes between 40 and 10 km for HCFC-22. Positive sign means displacement towards the satellite.

Height	FWHM	Displacement
40 km	554 km	−121 km
35 km	549 km	5 km
30 km	528 km	62 km
25 km	521 km	55 km
20 km	608 km	90 km
15 km	300 km	133 km
10 km	327 km	126 km

ACPD
15, 14783–14841, 2015

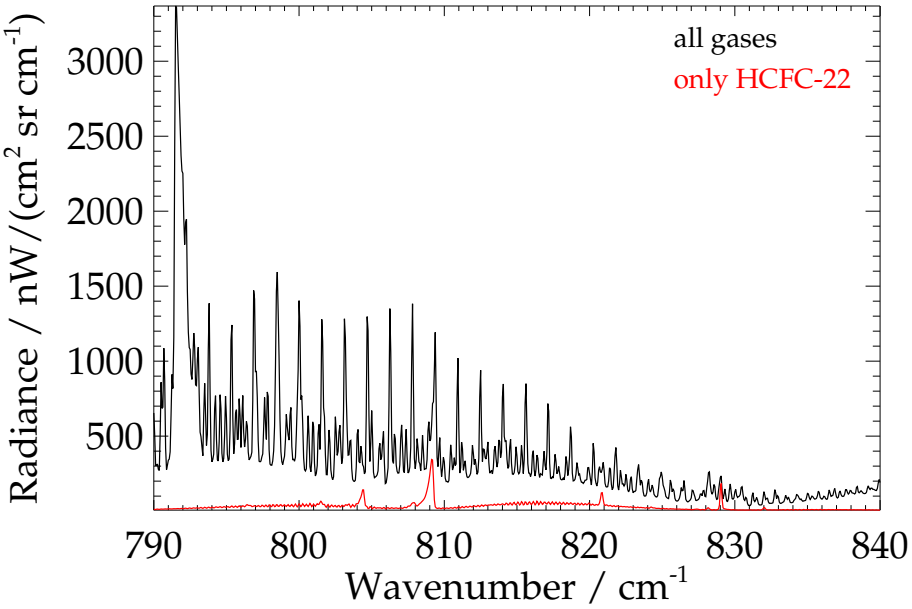

Figure 1. Typical spectrum of HCFC-22 (red curve) and combined spectrum of 24 gases (HCFC-22 included) (black curve) at 16 km tangent altitude.

ACPD
15, 14783–14841, 2015

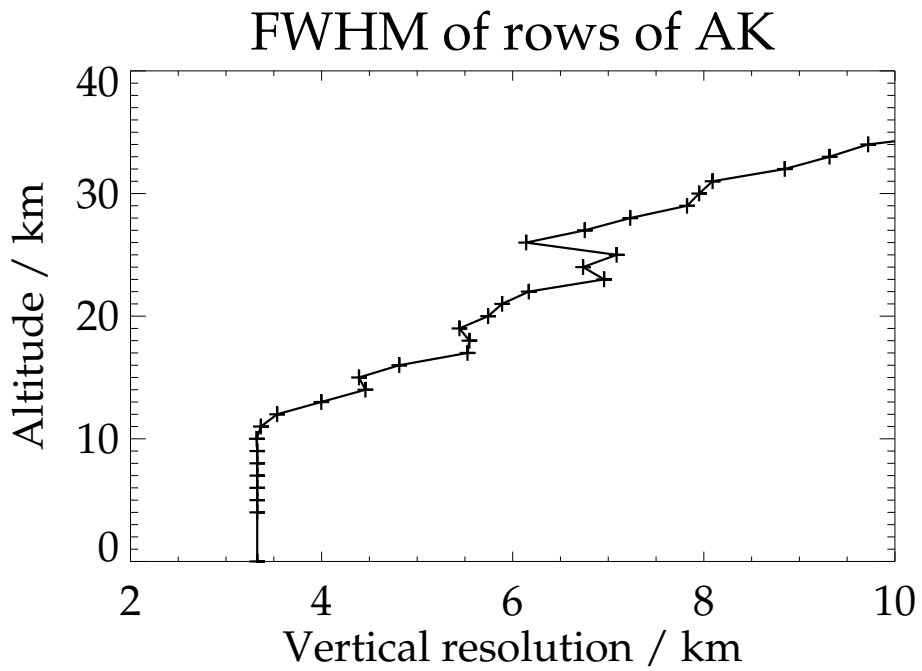

Figure 2. Altitude resolution in terms of full width at half maximum (FWHM) of a row of the averaging kernel matrix.

ACPD
15, 14783–14841, 2015

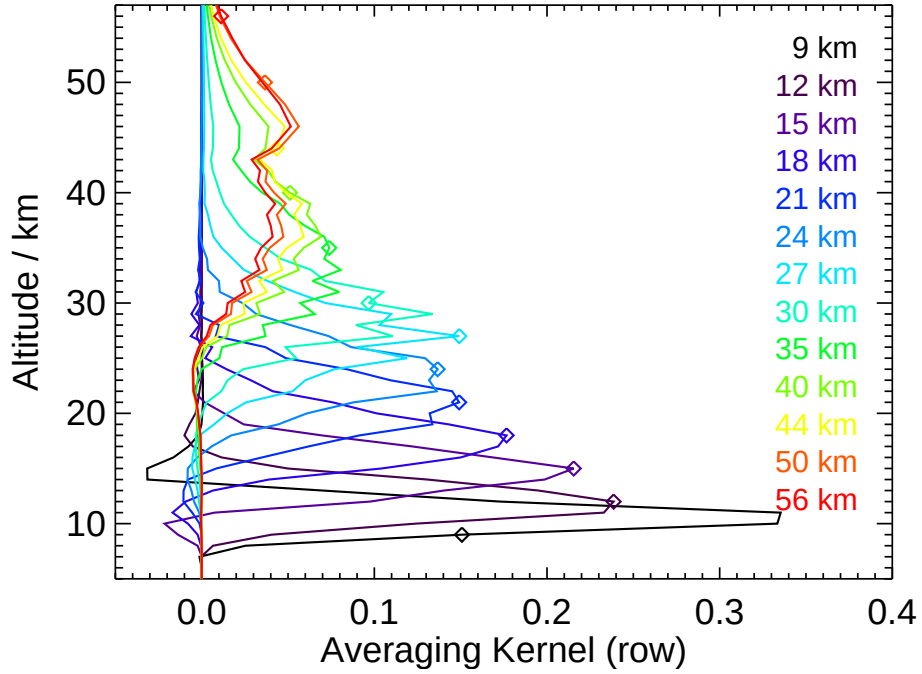

Figure 3. Rows of averaging kernel of HCFC-22 measurements for reduced spectral resolution nominal mode. The diamonds represent the nominal altitudes (e.g. the diagonal value of the averaging kernel matrix). For clarity, only every third kernel is shown.

ACPD
15, 14783–14841, 2015

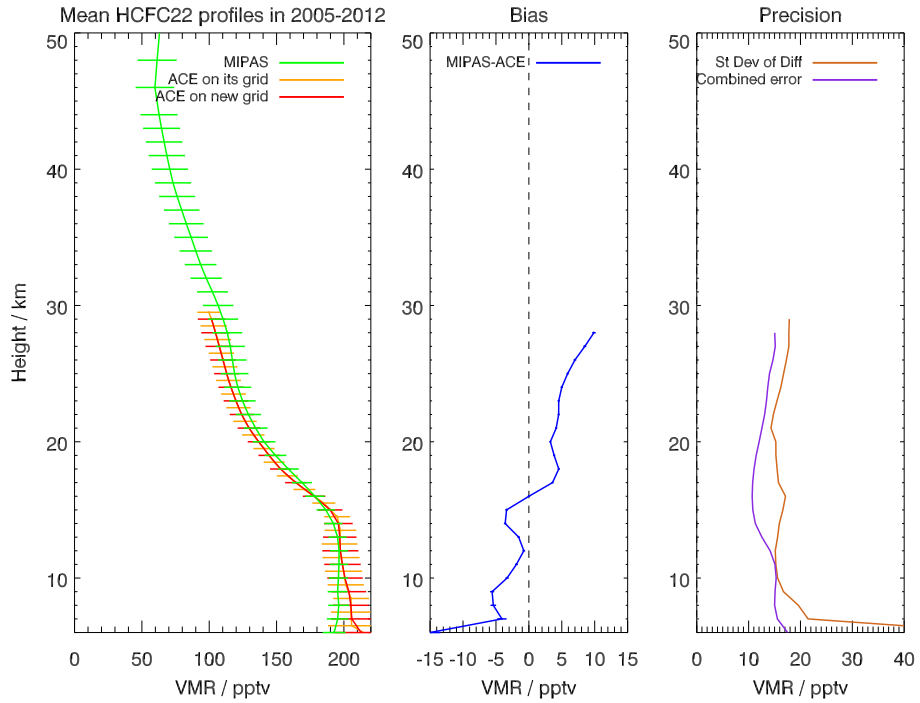

Figure 4. Mean profiles, bias, and standard deviation of the differences vs. estimated combined retrieval error for ACE-FTS and MIPAS retrievals of HCFC-22. The original altitude grid on which the ACE-FTS data were provided uses the same grid spacing as MIPAS of 1 km, but was shifted by 0.5 km. Thus, the data were resampled on the MIPAS grid.

ACPD
15, 14783–14841, 2015

Global HCFC-22 climatology from MIPAS

M. Chirkov et al.

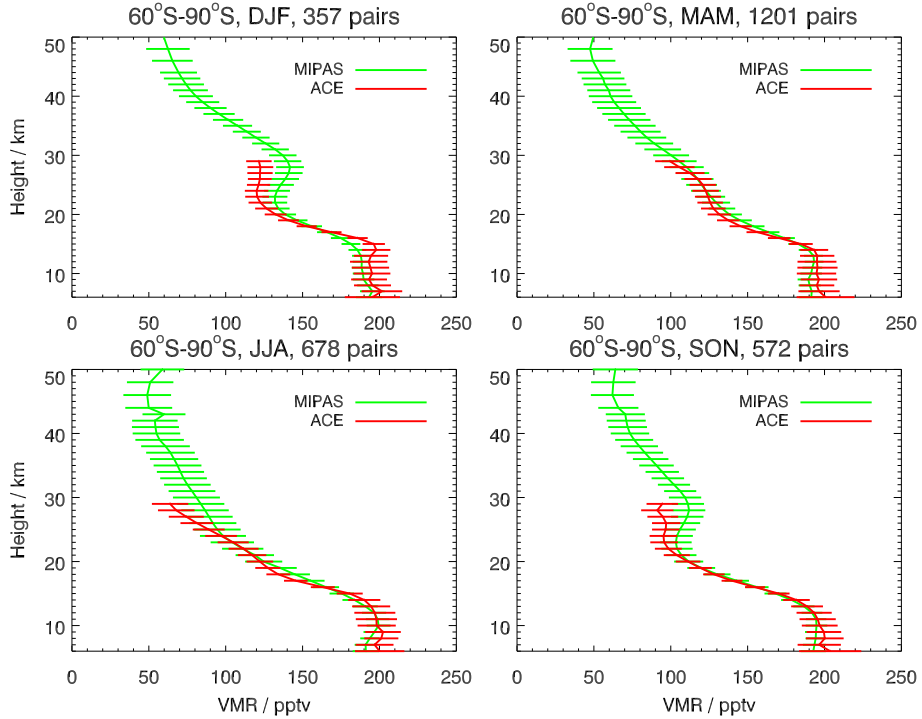

Figure 5. Seasonal mean vmr values (in pptv) of ACE-FTS (red) and MIPAS (green) in 2005–2012 at southern polar latitudes.

ACPD
15, 14783–14841, 2015

Global HCFC-22 climatology from MIPAS

M. Chirkov et al.

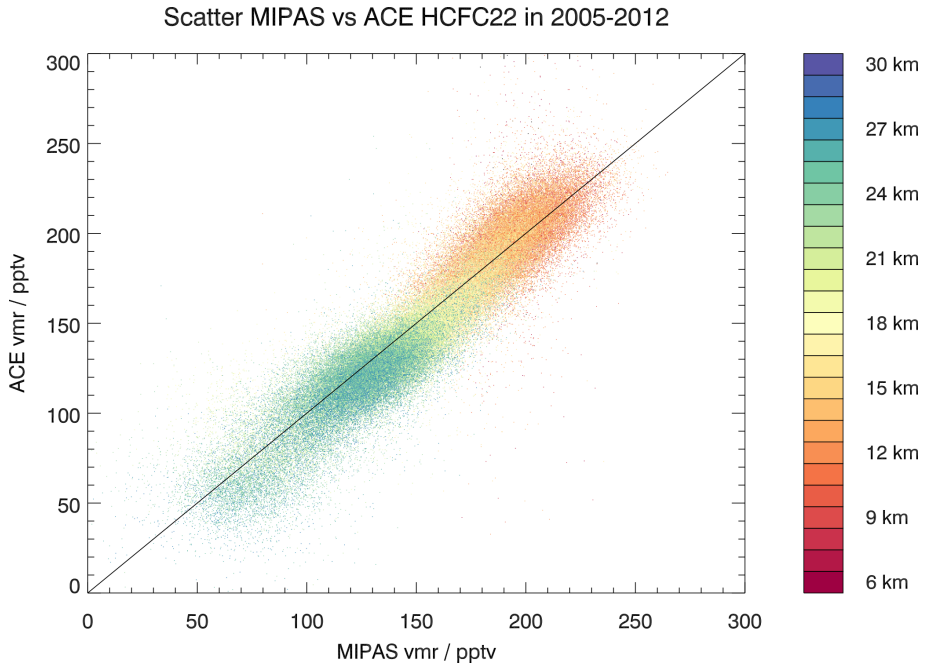

Figure 6. Scatter plot of ACE-FTS vs. MIPAS HCFC-22 data points.

ACPD
15, 14783–14841, 2015

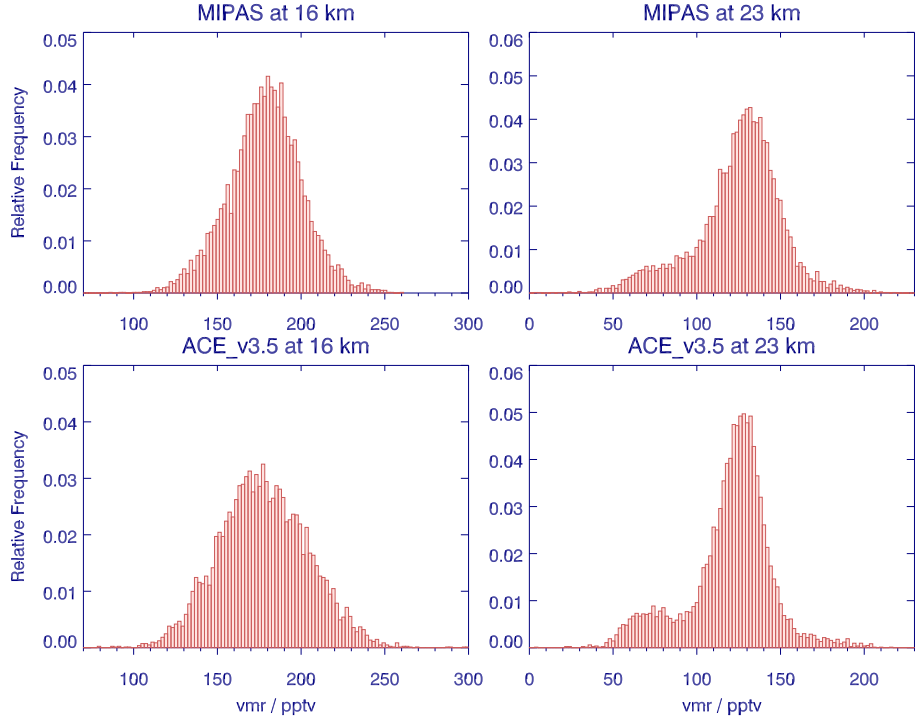

Figure 7. Histograms of MIPAS (upper panels) vs. ACE-FTS (lower panels) HCFC-22 mixing ratios at 16 km (left panels) and 23 km (right panels) altitude.

ACPD
15, 14783–14841, 2015

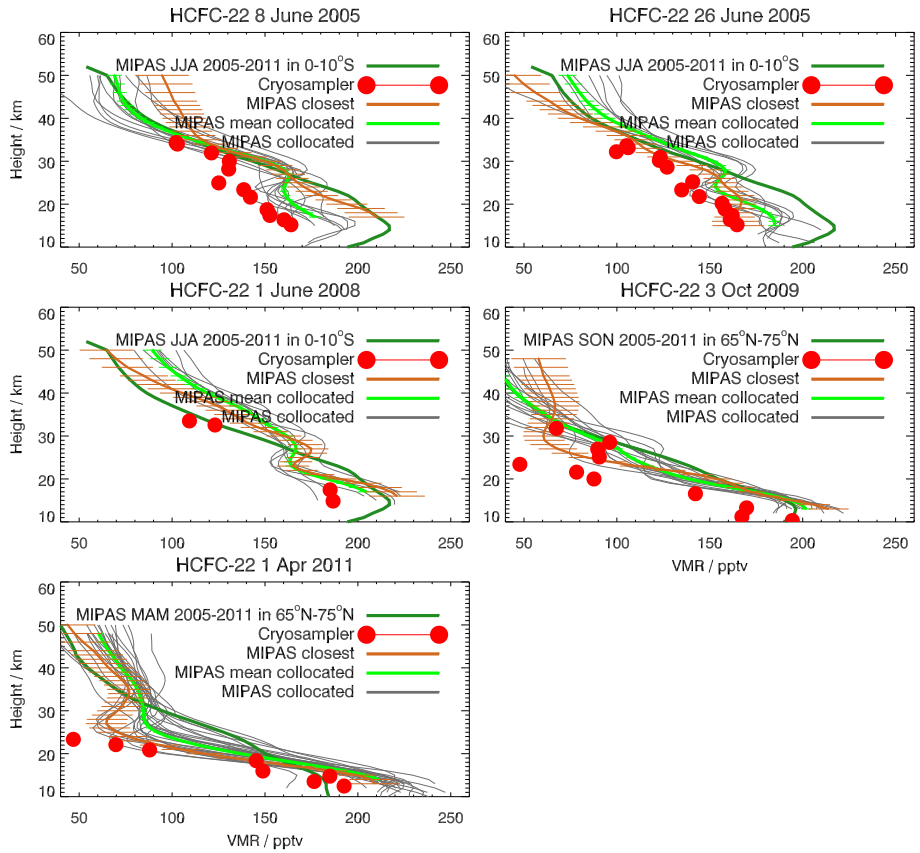

Figure 8. Five cryosampler profiles and MIPAS HCFC-22 vmr profiles – collocated, monthly and seasonal means in corresponding latitude bands.

ACPD
15, 14783–14841, 2015

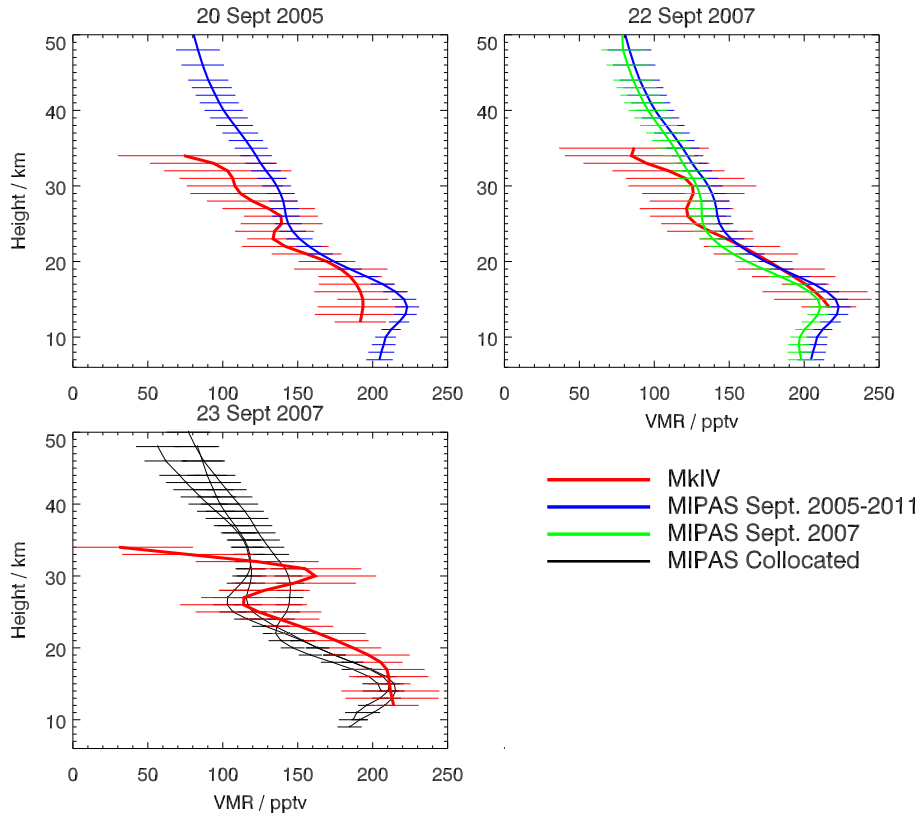

Figure 9. MkIV profiles and MIPAS HCFC-22 collocated, monthly and seasonal mean vertical profiles. The means are taken in the 30–40° N latitude band where the three balloon flights took place.

ACPD
15, 14783–14841, 2015

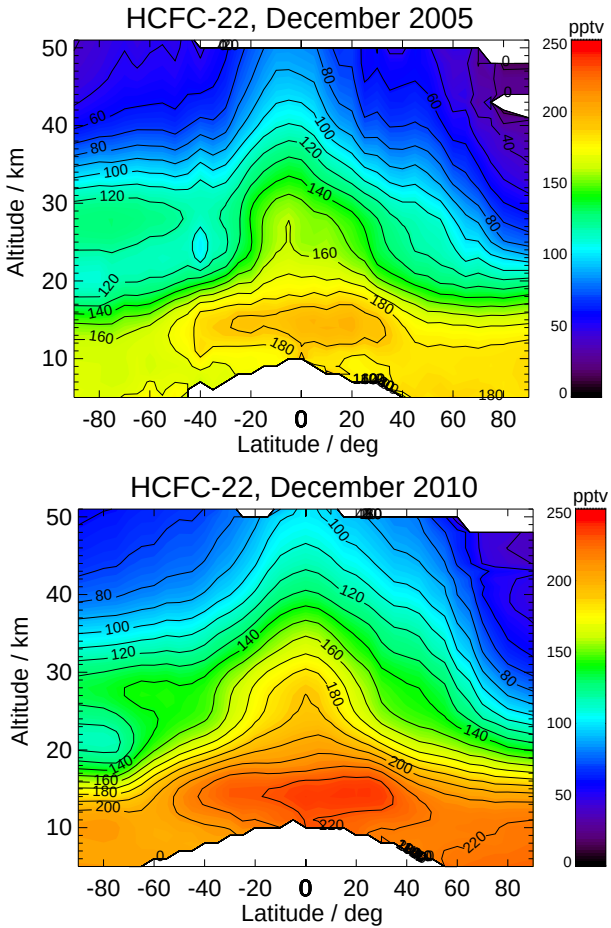

Figure 10. Monthly zonal means of HCFC-22 volume mixing ratios from 5 to 50 km for December 2005 (top) and December 2010 (bottom). The months have been selected to be approximately in the same QBO phase.

ACPD
15, 14783–14841, 2015

Global HCFC-22 climatology from MIPAS

M. Chirkov et al.

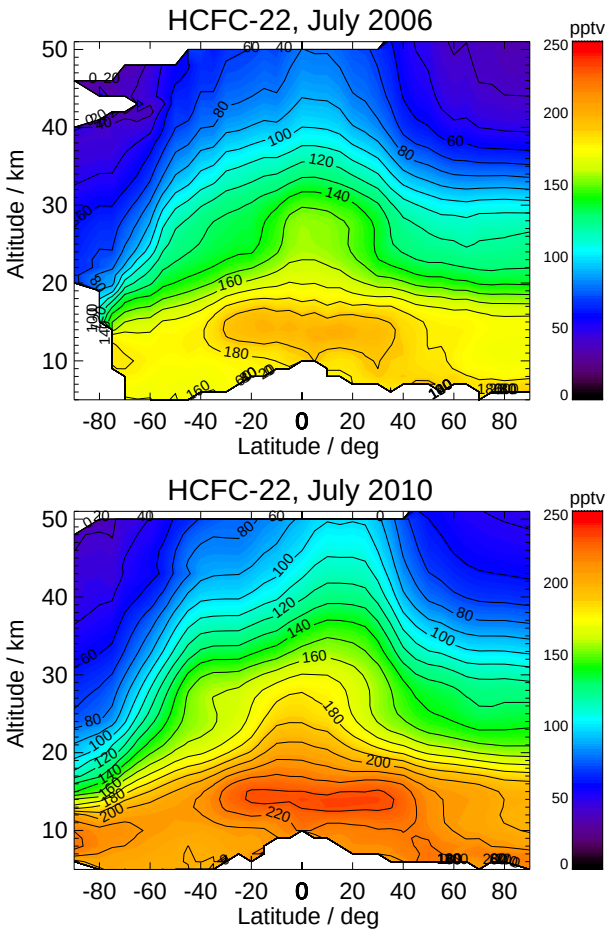

Figure 11. Same as Fig. 10, but for July 2006 (top) and 2010 (bottom).

ACPD
15, 14783–14841, 2015

Global HCFC-22 climatology from MIPAS

M. Chirkov et al.

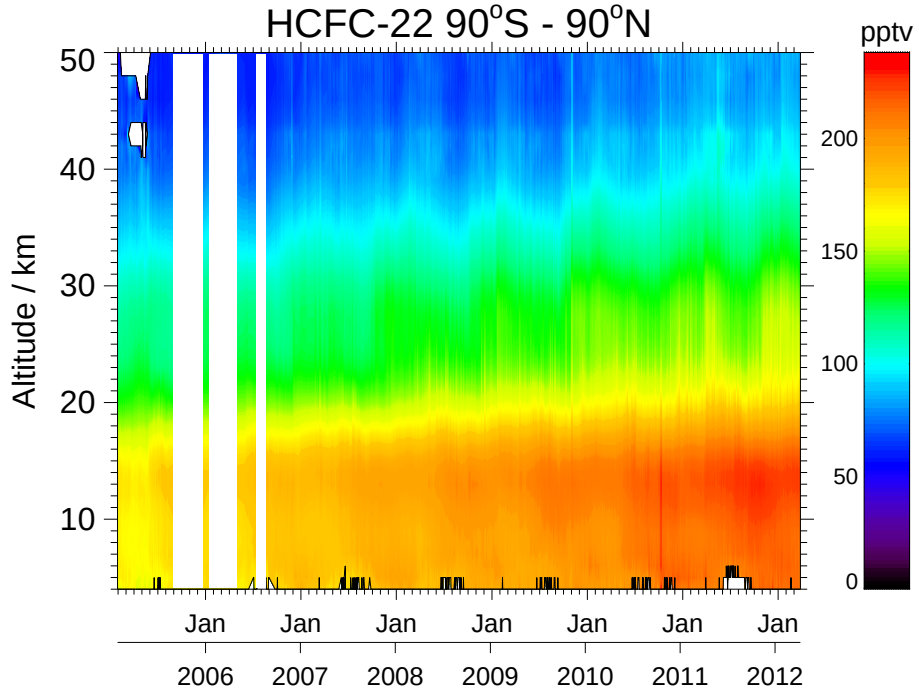

Figure 12. The globally averaged time series of HCFC-22 volume mixing ratio from January 2005 to April 2012.

ACPD
15, 14783–14841, 2015

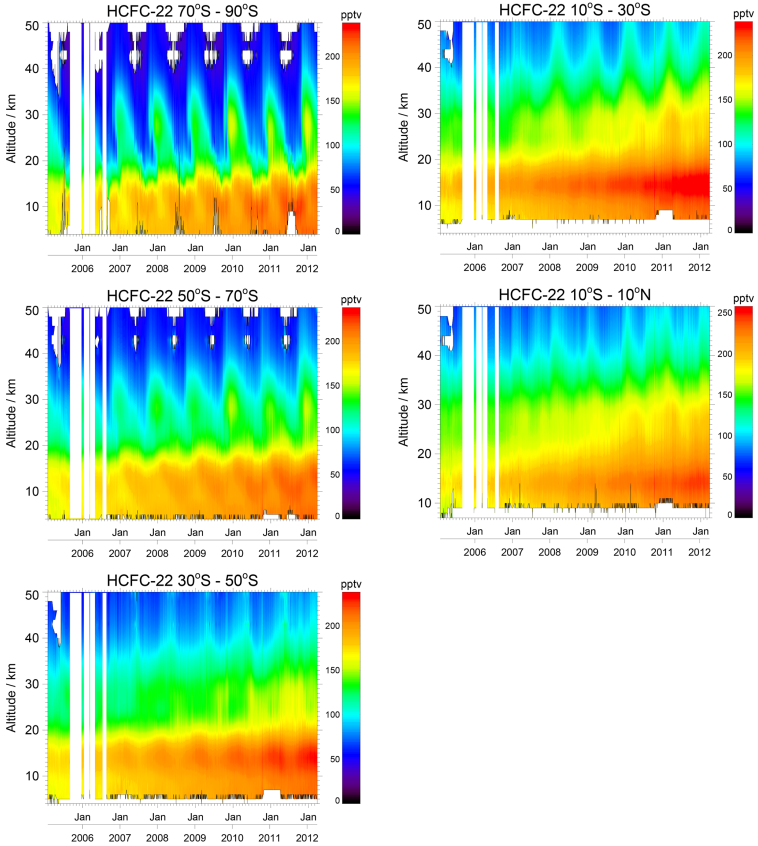

ACPD
15, 14783–14841, 2015

Global HCFC-22 climatology from MIPAS

M. Chirkov et al.

Figure 13. Time series of HCFC-22 vmrs from January 2005 to April 2012 for 70 to 90° S, 50 to 70° S, 30 to 50° S (left column, from top to bottom), 10 to 30° S, and 10° S to 10° N (right column, from top to bottom), generated from daily zonal means. White areas in the plots represent MIPAS data gaps. At low altitudes these are caused by clouds, while at high altitudes they are caused by a too low sensitivity of MIPAS. Data gaps covering all altitudes are associated with times when MIPAS did not measure.

ACPD
15, 14783–14841, 2015

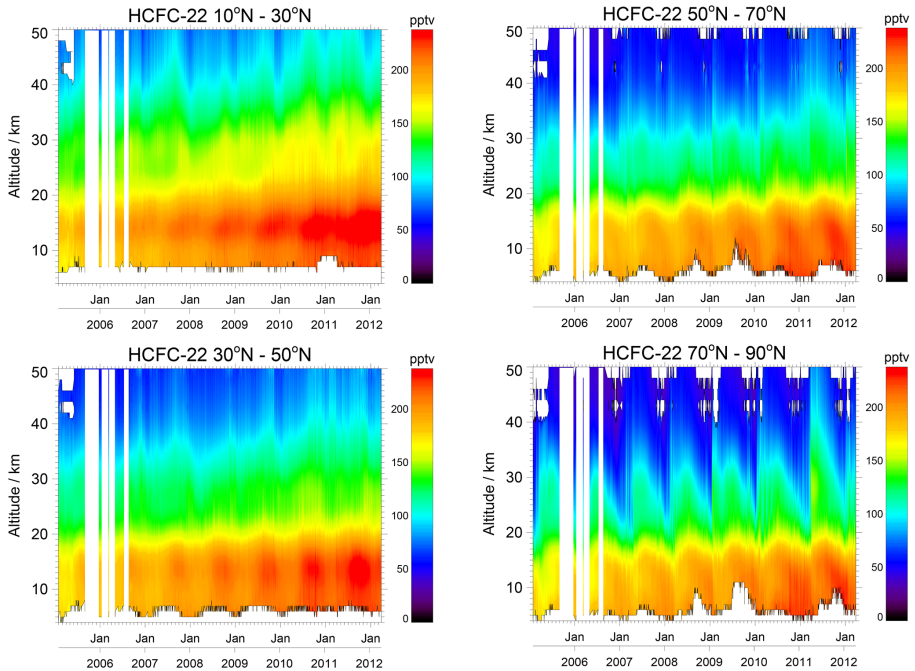

Figure 14. As Fig. 13, 10 to 30° N (top left), 30 to 50° N (bottom left), 50 to 70° N (top right), and 70 to 90° N (bottom right).

ACPD
15, 14783–14841, 2015

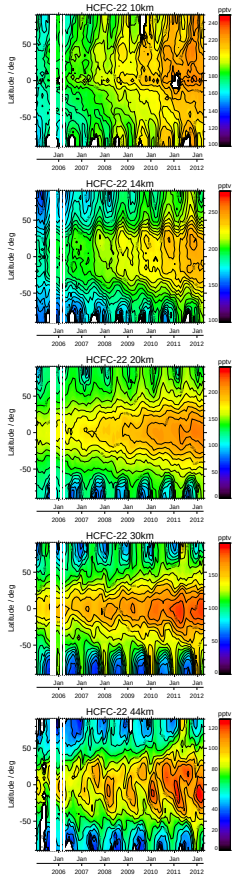

Figure 15. Latitude–time cross sections of HCFC-22 vmrs from January 2005 to April 2012 for altitudes of (from top to bottom) 10, 14, 20, 30, and 44 km, generated from monthly zonal mean data. Note different colour bars for different panels.

ACPD
15, 14783–14841, 2015

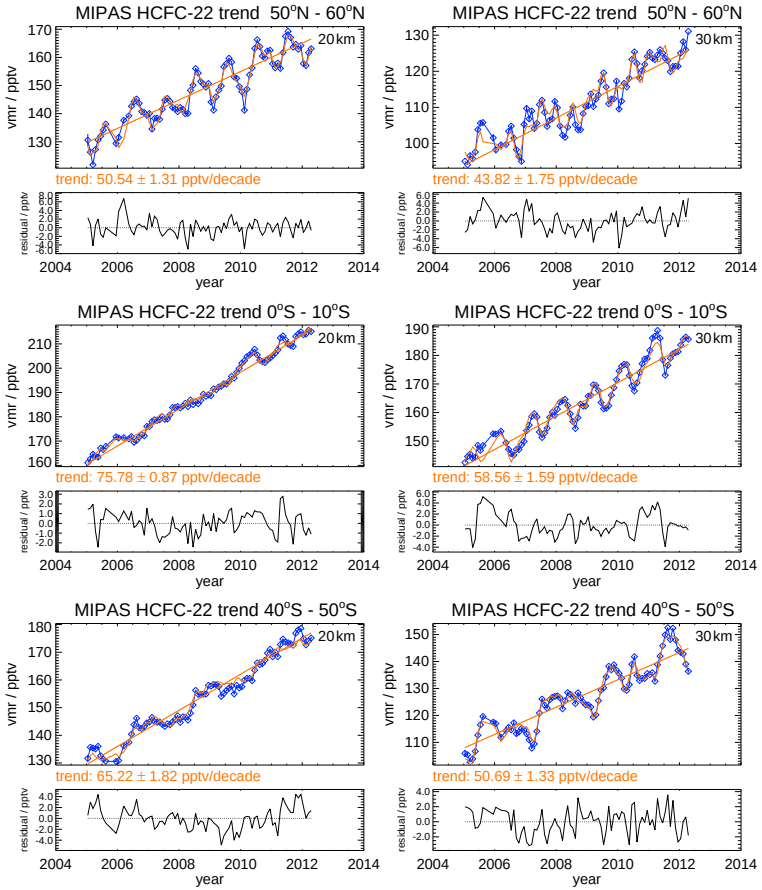

Figure 16. Time series of HCFC-22 volume mixing ratios (blue symbols) and their fits with the regression function described in the text (orange curves) at 20 km (left) and 30 km (right) altitude in three latitude bins. The linear trend component of the multi-parameter fit (straight orange line) is also shown.

ACPD
15, 14783–14841, 2015

Global HCFC-22 climatology from MIPAS

M. Chirkov et al.

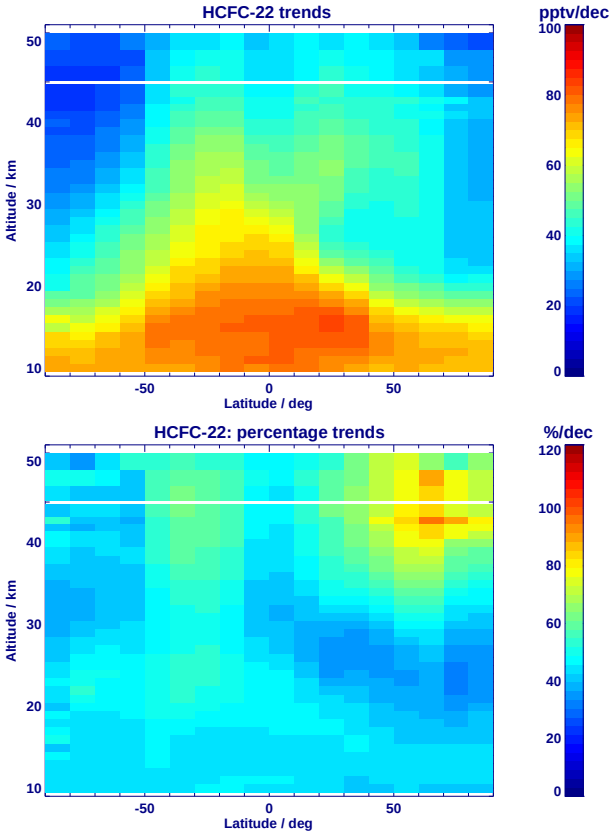

Figure 17. Trend of HCFC-22 volume mixing ratio for all latitude/altitude bins, in absolute units (pptv/decade) (top) and as percentage per decade relative to the background distribution in 2005 (i.e. the constant term of the regression analysis, see Eq. 1) (bottom). For the trends, autocorrelations have been considered in the fit.

ACPD
15, 14783–14841, 2015

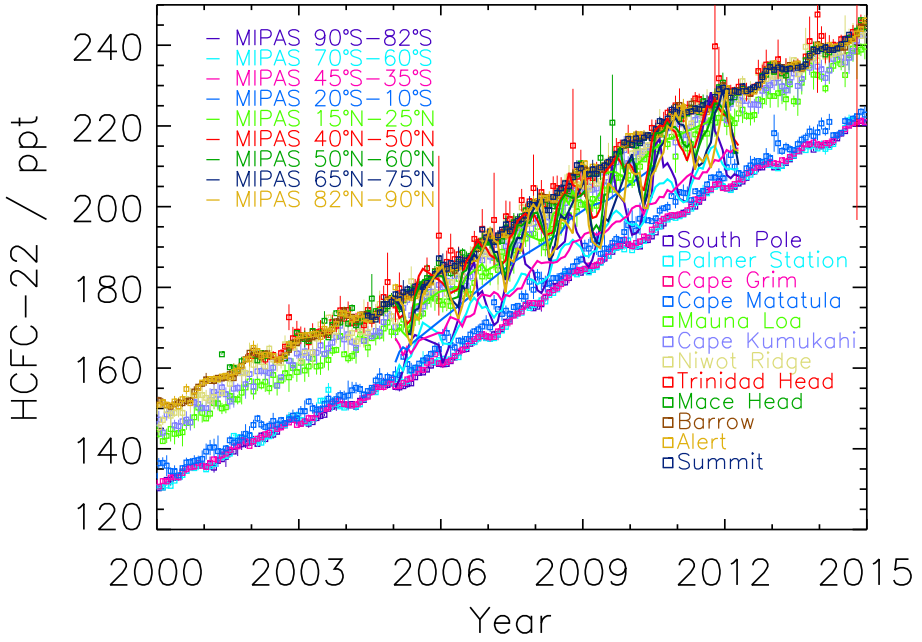

Figure 18. Comparison of HCFC-22 time series from several stations of the NOAA/GMD program with corresponding MIPAS values. Open squares: NOAA/GMD monthly mean data from several stations (see legend for color code); solid lines without symbols: MIPAS monthly mean data for 10° latitude bands around the respective station latitude; the color coding matches that of the stations.

ACPD
15, 14783–14841, 2015

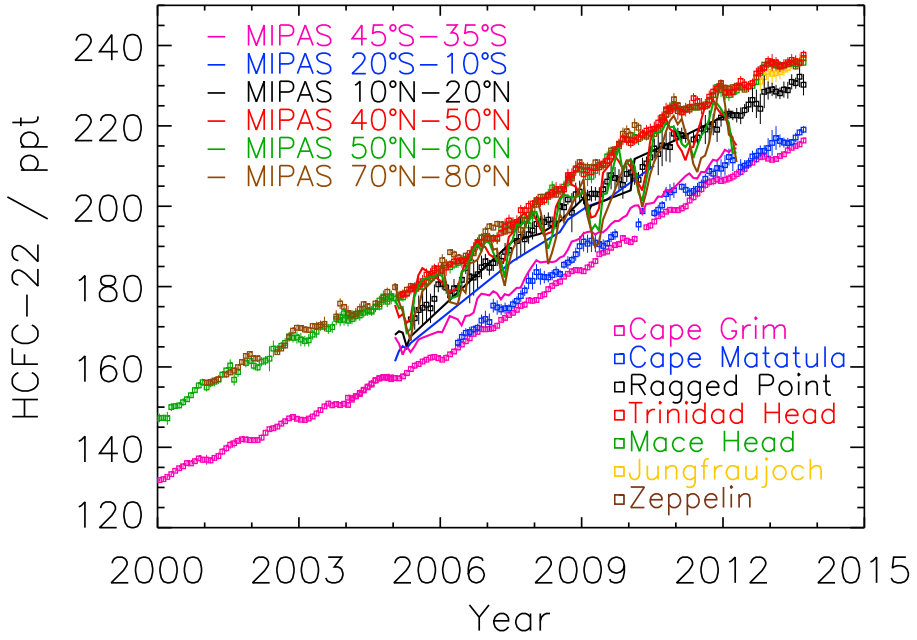

Figure 19. Comparison of HCFC-22 time series from seven AGAGE stations (open squares) taken from http://agage.eas.gatech.edu/data.htm with MIPAS HCFC-22 averages below 10 km for related latitude bands of 20–10° S (blue), 45–35° S (pink), 10–20° N (black), 40–50° N (red), 50–60° N (green), and 70–80° N (brown) (solid lines without symbols). The latitude bands are selected to include the latitude of the station with the respective color.

ACPD
15, 14783–14841, 2015

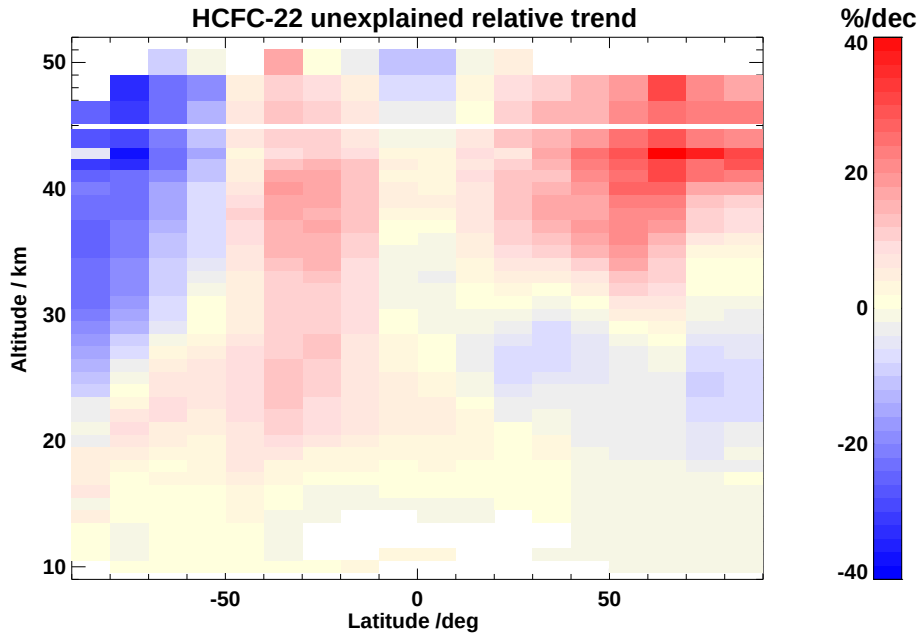

Figure 20. Differences between MIPAS stratospheric relative trends (referenced to the HCFC-22 background distribution in 2005, i.e. the constant term of the regression analysis (see Eq. 1)) and relative trends at ground measured by the NOAA/GMD program (global means), the latter corrected for the time lag between the air parcels' start in the troposphere and its arrival in the stratosphere.

ACPD
15, 14783–14841, 2015